Magnetic susceptibility of diluted magnetic semiconductors

Effects of positional disorder of the magnetic impurities

by

Adel Kassaian

A THESIS SUBMITTED IN PARTIAL FULFILMENT OF
THE REQUIREMENTS FOR THE DEGREE OF

MASTER OF SCIENCE

in

THE FACULTY OF GRADUATE STUDIES

(Department of Physics and Astronomy)

We accept this thesis as conforming
to the required standard

THE UNIVERSITY OF BRITISH COLUMBIA

July 30, 2004

Library Authorization

In presenting this thesis in partial fulfillment of the requirements for an advanced degree at the University of British Columbia, I agree that the Library shall make it freely available for reference and study. I further agree that permission for extensive copying of this thesis for scholarly purposes may be granted by the head of my department or by his or her representatives. It is understood that copying or publication of this thesis for financial gain shall not be allowed without my written permission.

ADEL KASSAIAN — Name of Author *(please print)*

29/07/2004 — Date (dd/mm/yyyy)

Title of Thesis: Magnetic susceptibility of diluted magnetic semiconductors
Effects of positional disorder of the magnetic impurities

Degree: Master of Physics Year: 2004

Department of Physics And Astronomy
The University of British Columbia
Vancouver, BC Canada

Abstract

In this thesis we investigate the magnetic properties of (III,Mn)V diluted magnetic semiconductors in the low carrier concentration regime. Variational and perturbative methods are applied to an impurity-band model, in order to derive approximation schemes for computation of the dynamical and the static magnetic susceptibilities. Based on these, we carry out numerical simulations which allow us to investigate the effects of positional disorder of the Mn atoms on the magnetic properties of the system. The magnetic susceptibilities are shown to depend sensitively on the amount of positional disorder. The results we obtain are consistent with previous studies of the spin wave spectrum and of the inhomogeneous ferromagnetic state of these materials.

Contents

List of Figures

Acknowledgements

I would like to thank my supervisor, Dr. Mona Berciu, for all her invaluable help and support. Her perpetual encouragement and instructive guidance have been the true engine of my endeavors. I would also like to thank my parents for their great help and their unconditional support through out my life.

Chapter 1

Introduction

Diluted magnetic semiconductors (DMSs) are a new class of materials obtained by doping an ordinary semiconductor with transition metals [1]. $Ga_{1-x}Mn_xAs$ is the most widely studied alloy of this group, since it has the highest reliable critical temperatures recorded to date: 150K for bulk samples with $x = 0.05$ [2] and 172K in digitally doped heterostructures [3]. In $Ga_{1-x}Mn_xAs$, substitution of a fraction x of the Ga atoms by Mn impurities introduces both localized Mn spins ($S = 5/2$) and holes into the system. The exchange interaction between the holes' spins and the Mn moments are known to be anti-ferromagnetic. They give raise to hole-mediated ferromagnetic interactions between Mn spins, leading to a ferromagnetic state below the critical temperature T_c. The interest in these materials is high due to their potential use of the spin degree of freedom in electronic devices. Concept devices have already been demonstrated, including spin-polarized light emitters [4] and electrically controlled ferromagnetism [5].

The magnetic properties of DMS have stimulated considerable theoretical interest in describing the physics of ferromagnetism. It is widely accepted that magnetization is due to charge-carrier mediated, effectively ferromagnetic, interactions between the Mn spins. It is also known experimentally that these alloys are heavily compensated, with hole concentrations much smaller than the Mn concentration, $c_h = p\, c_{Mn}$, $p = 10 - 30\%$ [6]. DMSs are alloy systems, with inherent positional disorder of Mn atoms. The spin-orbit coupling may also play a significant role in determining their properties. A theoretical treatment which takes into account all these factors and their effects on magnetic and transport properties of DMSs is not yet available. Instead, theoretical models have tended to concentrate on different aspects of the problem. The main trend that all theories agree on is that for low x and low carrier concentrations, T_c monotonically increases with increasing x and increasing hole concentration.

The model we study in this thesis is an impurity band model [7]. It is expected to be (at least qualitatively) valid at low concentrations, below and near the metal-insulator transition. Low carrier concentration implies a long screening length for Coulomb interactions, opening up the possibility that holes are moving in an impurity band through hopping processes. The relatively few holes in this system are expected to first occupy states in such an impurity band located above the valence band (the existence of the valence band is neglected in the model we use). Experimentally, the presence of an impurity band at low doping concentration x has been confirmed in photoemission measurements, which show the Fermi energy to lie in an impurity band inside the gap, for $x = 0.035$ [8]. Conductivity measurements at low temperatures also reveal Mott variable-rang hopping behavior [9, 10].

The low x in bulk DMS suggests that there are likely to be large spatial fluctuations in the magnetic properties due to spatial disorder of Mn ions positions. An impurity band model has the ability to study this type of disorder, unlike models which assume that the carriers occupy states in the valence band – this automatically implies translational symmetry and homogenous distribution of the holes throughout the whole system. Theoretical studies of this impurity-band model have shown that at low concentrations, positional disorder has significant effects on the magnetic properties of the system. It was shown that disorder increases the critical temperature [7, 11]. It also leads to an inhomogeneous ferromagnetic state which can be characterized by weakly interacting Mn spins residing in low density regions which are practically devoid of holes, and strongly coupled Mn spins in the high density regions where the holes are located with large probability. The signature of such inhomogeneity should be seen in magnetic observables such as magnetic susceptibilities. In this thesis, we study static and dynamical magnetic susceptibilities and investigate the effect of positional disorder on their behavior.

The thesis is organized as follows: in Chapter 2, we introduce the model and discuss typical parameter values. In Chapter 3, the Hartree-Fock approximation and its self-consistent solution are reviewed. Chapter 4 has two sections. The first is devoted to a derivation of the Random Phase Approximation (RPA) equations which allow the computation of the transverse dynamical susceptibility at both zero and finite temperatures. The second section introduces the formalism for the calculation of the static longitudinal susceptibility using perturbative methods. The numerical and analytical results for these susceptibilities are presented in the following two chapters. Chapter 5 describes the results for an ordered configuration of Mn spins, while in Chapter 6 we study the effects of positional disorder on the magnetic response functions. Finally, in Chapter 7 we summarize our results.

Chapter 2

The model

The electronic configuration of Mn is $3d^5 4s^2$. According to Hund's rule, each Mn has a spin $-\frac{5}{2}$ from its half-filled 3d shell. This is the largest possible spin for a partially filled $3d$ shell, and explains why Mn is currently the magnetic dopant of choice. When doped into a III-V semiconductor such as GaAs, the valence-II Mn substitutes for the valence-III element (Ga). It therefore acts as an acceptor and introduces a charge carrier (hole) in the system. This implies that the concentration of charge carriers should equal the concentration of magnetic moments (Mn spins) in such systems. However, experimentally it is found that the hole concentration is considerably smaller – as little as 10-30% of the Mn spin concentration – due to compensation centers, such as Mn interstitials or As antisites [1, 12]. The magnetic properties of the DMS are due to the exchange interactions between the Mn spins and the charge carrier spins. This interaction is known to be antiferromagnetic (AFM) [13].

All throughout this thesis we use an impurity-band model [7, 11, 14, 15] to investigate magnetic properties of the DMS materials. This model is justified near and below the metal-insulator transition ($x \approx 0.03$) where the density of charge carriers is not large enough to effectively screen the attractive Coulomb potential of the Mn dopants. As a result, bound impurity states are created about each Mn site, at an energy $E_b = 1$ Ry (= 112.4 meV, for Mn in GaAs [13]) above the top of the valence band. Due to interactions and wave-functions overlap, these impurity states broaden into an impurity band, and the holes first occupy states in this band. Only if the concentration of holes (or the temperature) is large enough, are states in the valence band itself occupied by holes. However, since the hole concentration is so small, we do not need to explicitly include the valence band states in our model.

Although the charge carriers are holes, in the following we perform a particle-hole transformation and use an electron-formalism to analyze this system. In other words, we in fact study an equivalent system doped with hypothetical donors, with impurity levels below a conduction-like band, instead of above a valence-like band. We also make the simplifying assumption that the isolated impurity wave-function for a charge carrier trapped near a Mn is a $1s$ hydrogen orbital. This approach neglects both the complicated orbital form of the acceptor wave-function (Ref. [13]) and the effects of the spin-orbit coupling. The former is not expected to lead to any qualitative changes. It has recently been proposed that spin-orbit coupling leads to frustration in the magnetic ordering by creating anisotropy in the magnetic exchanges [16]. However, subsequent work has raised doubts about the importance of anisotropy effects in such systems [17, 18]. Such effects are not included in the present study.

The III-V host semiconductor is assumed to have the zinc-blende structure appropriate for GaAs. N_d Mn dopants are placed at positions $\vec{R}_i$, $i = 1, ..., N_d$ on the $N \times N \times N$ FCC Ga sublattice, of lattice constant a ($a = 5.65$ $\mathring{A}$ for GaAs), corresponding to a doping $x = N_d/4N^3$. The number of charge carriers is fixed to $N_h = pN_d$, where we take $p = 10\%$. All throughout this paper, we assume periodic boundary conditions. We investigate the Hamiltonian

$$\mathcal{H} = \sum_{i,j,\sigma} t_{ij} c^\dagger_{i\sigma} c_{j\sigma} + \sum_{i,j} J_{ij} \vec{S}_i \cdot \vec{s}_j. \tag{2.1}$$

Here, $c^\dagger_{i\sigma}$ creates a charge carrier with spin σ in the impurity state centered at site $\vec{R}_i$. The first term describes the hopping of charge carriers between impurity states. We use the parameterization $t_{ij} = 2(1 + r/a_\mathrm{B}) \exp(-r/a_\mathrm{B})$ Ry, where $r = |\mathbf{R}_i - \mathbf{R}_j|$, of magnitude and form appropriate for hopping between two isolated $1s$ impurities which are not too close to one another [19]. For Mn in GaAs, the Bohr radius is $a_B \approx 8\mathring{A}$ [7, 13]. This hopping term has been shown to lead to the appearance of an impurity band which has a mobility edge, as well as a characteristic energy for the occupied states in agreement with physical expectation [11, 21].

The second term of the Hamiltonian (2.1) describes the AFM exchange between the Mn spin $\vec{S}_i$ and the charge carrier spin $\vec{s}_j = \frac{1}{2} c^\dagger_{j\alpha} \vec{\sigma}_{\alpha\beta} c_{j\beta}$, where $\vec{\sigma}$ are the Pauli spin matrices. This AFM exchange is proportional to the probability of finding the charge carrier trapped at $\vec{R}_j$ near the Mn spin at $\vec{R}_i$, and therefore $J_{ij} = J|\phi_j(\vec{R}_i)|^2 = J \exp\left(-2|\vec{R}_i - \vec{R}_j|/a_B\right)$. Based on calculations of the isolated Mn impurity in GaAs, we estimate the exchange coupling between a hole and its trapping Mn ($\vec{R}_i = \vec{R}_j$) to be $J = 15$ meV [7, 13].

Chapter 3

The Hartree Fock Approximation

As the first step and a basis for other approximations, we need to find the self-consistent mean-field solution of Hamiltonian (2.1). The detailed study of the mean-field approximation for this Hamiltonian has been performed in Refs. [7, 11]. In this section we derive the main results using the density matrix variational approach, which consists in expressing and then minimizing the thermodynamic potential of the system with respect to a trial density matrix.

For the Hamiltonian (2.1) we use a variational Hartree-Fock Hamiltonian $\hat{\mathcal{K}}$ consisting of one-body fermionic operators and non-interacting Mn spins. We assume the symmetry is spontaneously broken in the z-direction:

$$\hat{\mathcal{K}} = \sum_{ij,\sigma} h_{ij,\sigma} c^{\dagger}_{i\sigma} c_{j\sigma} - \sum_{i} H_i S^z_i \tag{3.1}$$

The most general variational form for the mean field Hamiltonian would allow spin flips $\sum_{i,j,\sigma} h_{i\alpha,j\beta} c^{\dagger}_{i\alpha} c_{j\beta}$ for the fermionic part and magnetic non-collinearity $\sum_i \vec{H}_i \cdot \vec{S}_i$, for the Mn spin part of $\hat{\mathcal{K}}$. However, a previous study of this model [11] showed that the self-consistent mean-field ground state is always collinear, implying that the variational guess of Eq. (3.1) is appropriate.

The thermodynamic potential (the free energy) can be shown to satisfy the variational principle [22],

$$\mathcal{F}_{eq} \leq \mathcal{F}(\hat{\mathcal{K}}) = -k_B T \ln \mathcal{Z}_0 + Tr\{\hat{\mathcal{D}}_0[\hat{\mathcal{H}} - \hat{\mathcal{K}}]\}. \tag{3.2}$$

Here, $\hat{\mathcal{D}}_0$ is our trial density matrix for the mean-field Hamiltonian $\hat{\mathcal{K}}$,

$$\hat{\mathcal{D}}_0 = \frac{e^{-\beta(\hat{\mathcal{K}} - \mu\hat{\mathcal{N}})}}{\mathcal{Z}_0}. \tag{3.3}$$

where $\hat{\mathcal{N}} = \sum_{i,\sigma} c^{\dagger}_{i\sigma} c_{i\sigma}$ is the particle number operator. $\mathcal{Z}_0$ is the corresponding grand-canonical partition function,

$$\mathcal{Z}_0 = Tr\, e^{-\beta(\hat{\mathcal{K}} - \mu\hat{\mathcal{N}})}. \tag{3.4}$$

The Hartree-Fock parameters $h_{ij,\sigma}$ and H_i are found from minimizing $\mathcal{F}(\hat{\mathcal{K}})$ [Eq. (3.2)]. We first define the expectation values:

$$\rho_{ji,\sigma} = Tr\{\hat{\mathcal{D}}_0 c^{\dagger}_{i\sigma} c_{j\sigma}\} = -\frac{1}{\beta} \frac{\partial \ln \mathcal{Z}_0}{\partial h_{ij,\sigma}} \tag{3.5}$$

$$\langle \vec{S}_i \rangle = S_{\rm Mn}(i)\hat{e}_z = Tr[\hat{\mathcal{D}}_0 \vec{S}_i]; \qquad S_{\rm Mn}(i) = -\frac{1}{\beta}\frac{\partial \ln \mathcal{Z}_0}{\partial H_i}, \tag{3.6}$$

It can be easily checked that $S_{\rm Mn}(i)$, the expectation value of the Mn spin at site i, is given by:

$$S_{\rm Mn}(i) = \frac{Tr\left\{S_i^z e^{-\beta\sum_i H_i S_i^z}\right\}}{Tr\left\{e^{-\beta\sum_i H_i S_i^z}\right\}} = B_S(\beta H_i). \tag{3.7}$$

where $B_S(x) = (S+\frac{1}{2})\coth[(S+\frac{1}{2})x] - \frac{1}{2}\coth\frac{x}{2}$ is the Brillouin function ($S = \frac{5}{2}$ for Mn). It should also be mentioned that $\rho_{jj,\sigma}$ is by definition the probability of finding a charge carrier with spin σ at site j. As a result, we must have:

$$\sum_{j,\sigma} \rho_{jj,\sigma} = N_h. \tag{3.8}$$

The functional $\mathcal{F}(\hat{\mathcal{K}})$ can be written in terms of $\rho_{ji,\sigma}$ and $S_{\rm Mn}(i)$ as:

$$\mathcal{F}(\hat{\mathcal{K}}) = -k_B T \ln \mathcal{Z}_0 + \sum_{ij,\sigma} t_{ij}\,\rho_{ji,\sigma} + \sum_{ij,\sigma} J_{ij} S_{\rm Mn}(i)\frac{\sigma}{2}\,\rho_{jj,\sigma}$$

$$- \sum_{ij,\sigma} h_{ij,\sigma}\,\rho_{ji,\sigma} + \sum_i H_i S_{\rm Mn}(i). \tag{3.9}$$

Its variation, $\delta\mathcal{F}$, can be expressed in terms of the variations of our trial density matrix parameters, δH_i and $\delta h_{ij,\sigma}$ which in turn imply changes in the expectation values $\delta S_{\rm Mn}(i)$ and $\delta\rho_{ji,\sigma}$:

$$\delta\mathcal{F} = \sum_i \delta S_{\rm Mn}(i)\left\{H_i + \sum_{j,\sigma} J_{ij}\frac{\sigma}{2}\rho_{jj,\sigma}\right\}$$

$$+ \sum_{ij,\sigma} \delta\rho_{ji,\sigma}\left\{t_{i,j} + \delta_{ij}\sum_k J_{ik} S_{\rm Mn}(k)\frac{\sigma}{2} - h_{ij,\sigma}\right\}. \tag{3.10}$$

The thermodynamic potential is minimized by setting $\delta F = 0$ and we find the self-consistent, mean-field equations to be given by:

$$H_i = -\sum_{j,\sigma} \frac{\sigma}{2} J_{ij}\rho_{jj,\sigma} \tag{3.11}$$

$$h_{ij,\sigma} = t_{ij} + \frac{\sigma}{2}\delta_{ij}\sum_k J_{ik} S_{\rm Mn}(k). \tag{3.12}$$

The first equation (3.11) simply states that the effective magnetic field acting on each Mn spin is induced by charge carriers through the AFM exchange interactions. The second equation (3.12) relates the mean-field fermionic Hamiltonian matrix elements to the kinetic terms t_{ij} coming from hopping and the

potential energy terms $\frac{\sigma}{2}\delta_{ij}\sum_k J_{ik}S_{\rm Mn}(k)$ arising from the AFM Heisenberg interaction with the spins of the Mn impurities.

In order to establish the procedure for determining the mean-field ground state self-consistently, we first diagonalize the fermionic contribution to the Hartree-Fock Hamiltonian $K_{el} = \sum_{i,j,\sigma} h_{ij,\sigma} c^{\dagger}_{i\sigma} c_{j\sigma}$. We use a unitary transformation of the charge-carrier operators:

$$a^{\dagger}_{n\sigma} = \sum_i \psi_{n\sigma}(i) c^{\dagger}_{i\sigma}, \tag{3.13}$$

and diagonalize the fermionic contribution to K such that we have:

$$K_{el} = \sum_{ij,\sigma} h_{ij,\sigma} c^{\dagger}_{i\sigma} c_{j\sigma} = \sum_{n\sigma} E_{n\sigma} a^{\dagger}_{n\sigma} a_{n\sigma}. \tag{3.14}$$

It follows easily from the unitary property of the transformation that

$$\sum_j h_{ij,\sigma}\psi_{n\sigma}(j) = \sum_j t_{ij}\psi_{n\sigma}(j) + \frac{\sigma}{2}\sum_k J_{ik}S_{\rm Mn}(k)\psi_{n\sigma}(i) = E_{n\sigma}\psi_{n\sigma}(i). \tag{3.15}$$

After solving this eigenequation, we can calculate $\rho_{jj,\sigma}$, defined in Eq. (3.5):

$$\rho_{jj,\sigma} = \sum_{n,m} \psi^{*}_{n\sigma}(j)\psi_{m\sigma}(j)\langle a^{\dagger}_{n\sigma} a_{m\sigma}\rangle = \sum_n f(E_{n\sigma})|\psi_{n\sigma}(j)|^2 \tag{3.16}$$

where $f(E_{n\sigma}) = [\exp(\beta(E_{n\sigma} - \mu)) + 1]^{-1}$ is the Fermi distribution. Eqs. (3.16) and (3.8) yield the equation for determining the chemical potential μ:

$$\sum_{n,\sigma} f(E_{n\sigma}) = N_h \tag{3.17}$$

As our last step, by using Eq. (3.16), we can rewrite Eq. (3.11) as:

$$H_i = -\sum_j J_{ij} s_h(j), \tag{3.18}$$

where $s_h(i)$ is the average spin created by charge carriers at site i, given by

$$s_h(i) = \frac{1}{2}\left(\rho_{ii,\uparrow} - \rho_{ii,\downarrow}\right) = \frac{1}{2}\sum_{n\sigma} \sigma\,|\psi_{n\sigma}(i)|^2 f(E_{n\sigma}) \tag{3.19}$$

These equations can be used as the iteration steps to determine the self-consistent mean fields and mean field ground state for a given temperature T. We start with an initial guess for the Mn spins at each site $S_{\rm Mn}(i)$ for a given temperature; we then use diagonalization [Eqs. (3.15), (3.12)] to find all the fermionic energies $E_{n\sigma}$ and wave functions $\psi_{n\sigma}(i)$. The chemical potential μ and charge carriers' spins $s_h(i)$ at each site are then determined from Eqs. (3.17) and (3.19). The effective fields H_i at each site can be derived using equations

(3.18) and the new values for $S_{\rm Mn}(i)$ are given by the Brillouin functions of Eq. (3.7). We repeat the iterations until the self consistency condition is reached. In this work we define self consistency by requesting that the variation between successive values of the average Mn spins be generally less than $\epsilon_{sc} = 10^{-4}$. Where needed, values for ϵ_{sc} as low as 10^{-6} shall be considered. The same self-consistent Hartree-Fock equations can be obtained if one starts from the mean-field factorized approximation for the Hamiltonian [7]:

$$\mathcal{H}^{HF} = \sum_{i,j,\sigma} t_{ij} c^{\dagger}_{i\sigma} c_{j\sigma} + \sum_{i,j} J_{ij} S_{\rm Mn}(i) \frac{\sigma}{2} c^{\dagger}_{j\sigma} c_{j\sigma} + \sum_{i,j} J_{ij} s_h(j) S^z_i. \qquad (3.20)$$

A detailed study of this mean-field approximation has been carried out in Ref. [11]. Here, we briefly review some important results which are relevant for the work we present in the following sections:

(1). In the limit $T \to 0$, irrespective of the positions of the Mn spins, the ground-state converges to a collinear ferromagnetic state, with Mn spins fully polarized in one direction ($+z$-axis) and charge carriers spins fully polarized in the opposite direction ($-z$-axis):

$$|\Psi\rangle_{cc} = \prod_{n=1}^{N_h} a^{\dagger}_{n\downarrow} |0\rangle$$

$$|S(1), \ldots, S(N_d)\rangle = |S, S, \ldots, S\rangle.$$

The reason for this is that at zero temperature there is a gap between the last occupied spin-down energy level and the first spin-up energy level, leading to full polarization of the charge carriers. In turn, through the AFM interactions, this induces an effective magnetic field in the opposite direction, acting on the Mn spins; as a result, all Mn spins become fully polarized as well. For $T = 0$, the mean-field ground state of the whole system can then be written as

$$|\Psi_0\rangle = \prod_{p=1}^{N_h} a^{\dagger}_{p\downarrow} |0\rangle \otimes |S, S, \ldots, S\rangle \qquad (3.21)$$

(2). We can compute the magnetization for any finite temperature using iterations, as explained earlier. We start the first iteration for the lowest temperature considered by assuming that all Mn spins are fully polarized, $S_{\rm Mn}(i) = \frac{5}{2}$. After several iterations, the self-consistent values $S_{\rm Mn}(i)$ corresponding to this temperature are found. We then use these values as the initial guess for the next higher temperature considered, etc. This allows us to find, at each finite temperature, the self-consistent solution with the highest possible total magnetization. A typical example of a magnetization curve as a function of temperature, for different levels of disorder, is shown in Fig. 3.1, for four different types of disorder realizations. In increasing order of T_c, the curves correspond to (i) a perfectly ordered Mn superlattice (which a superlattice constant of $3a$); (ii) weak disorder, corresponding to randomly displacing each Mn in (i) to one of

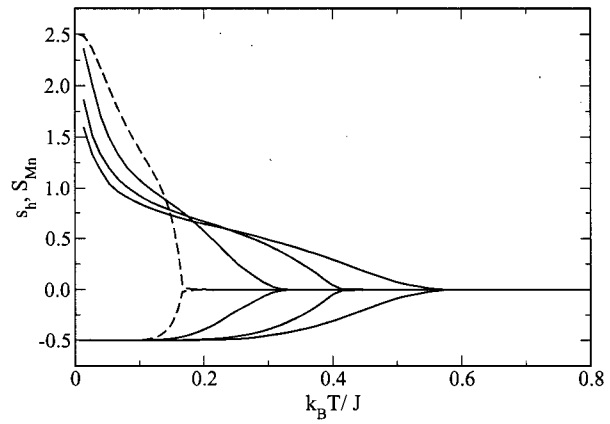

Figure 3.1: The average Mn spin $S_{\rm Mn}$ and carrier spins s_h, for $x = 0.00926$ and $p = 10\%$. In increasing order of T_c, the curves are for ordered, weakly disordered, moderately disordered and completely random distributions of Mn (from Ref. [7]).

the 12 nearest neighbor sites of the underlying FCC sublattice; (iii) moderate disorder, corresponding to a random distribution of Mn on the FCC sublattice, subject to the constraint that all Mn-Mn distances are greater than $2a$; (iv) completely random distribution of Mn on the FCC sublattice. Such curves show that disorder has a significant effect on the magnetic properties, changing both the critical temperature as well as the shape of the magnetization curve. The explanation for this behavior is simple: in the ordered system, invariance to translations insures that holes are homogeneously divided amongst all the Mn spins. By contrast, in the disordered sample, there are fluctuations in the local concentration of Mn spins. Here, the (relatively few) holes reside in the regions with higher Mn concentration, where they can more effectively lower their total energy by interacting with more spins. As a result, the effective magnetic fields H_i in these regions are much higher than in the ordered case, pushing the characteristic temperature where these regions become magnetized to higher temperature and increasing T_c. On the other hand, spins in the low concentration regions, which are devoid of holes, have extremely weak effective fields H_i and do not magnetize unless the temperatures are also low, $k_BT \sim H_i$. This explains why even at temperatures well below T_c there is still a sizable fraction of unpolarized spins.

Each magnetization curve shows three different regimes. The first regime is below a temperature we call T_p, where the charge carriers become "frozen" at the bottom of the $\sigma = \downarrow$ band (i.e. the charge carrier spins are fully saturated, $s_h = -1/2$). Below T_p, the Mn spins behave as if they are in a constant effective magnetic field [see Eq. (3.18)]. The second regime is $T_p < T < T_c$, where the holes begin to occupy some spin-up states, until they become completely

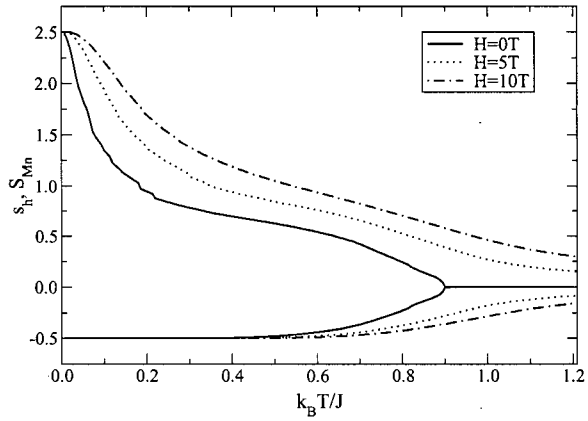

Figure 3.2: Mn and charge carrier average magnetizations as a function of T, for a random Mn configuration with $x = 0.05$ and $p = 10\%$, and external magnetic field $H = 0, 5$ and 10T. The overall magnetization is significantly increased at all T (from Ref. [11]).

unpolarized at $T = T_c$. Finally, the third regime is $T > T_c$ where both Mn and charge carrier spins are unpolarized.

(3). In Ref. [11] the effects due to addition of other terms to the Hamiltonian (2.1) have been considered. The term which is relevant to our work describes an external constant magnetic field which fixes the direction of magnetization. In this case the Hamiltonian becomes:

$$\mathcal{H} = \sum_{i,j,\sigma} t_{ij} c^{\dagger}_{i\sigma} c_{j\sigma} + \sum_{i,j} J_{ij} \vec{S}_i \cdot \vec{s}_j$$

$$-g\mu_B H \sum_i \frac{\sigma}{2} c^{+}_{i\sigma} c_{i\sigma} - \tilde{g}\mu_B H \sum_i S^z_i \tag{3.22}$$

The two new terms in Eq. (3.22) describe the interaction of the carrier and Mn spins with the external magnetic field H pointing in the z direction. It can be easily shown that its effect on the mean-field equations is to change Eqs. (3.11) and (3.12) into:

$$H^H_i = \tilde{g}\mu_B H - \sum_j J_{ij}\, s^H_h(j) \tag{3.23}$$

$$h^H_{ij,\sigma} = t_{ij} + \frac{\sigma}{2}\delta_{ij} \left[\sum_k J_{ik} S^H_z(k) - g\mu H \right]. \tag{3.24}$$

The upper index H distinguishes between the mean-field equations and solutions of the cases with and without external magnetic fields. We can find the

magnetization for any values of temperature and magnetic field through the same iterational procedure described before. The only differences are that we diagonalize the charge carrier Hamiltonian matrix (3.24) instead of Eq. (3.12) to find the energies and wave functions; and that we use Eq. (3.23) for the effective magnetic fields instead of Eq. (3.11) to calculate each $S_{\mathrm{Mn}}(i)$. The dependence of the average magnetization on temperature for values H=0, 5, 10T is shown in Fig. 3.2. We see that even though the external magnetic field is opposite to the holes' spins and we therefore might expect to see depolarization of the holes, instead they are getting even more polarized. This is because as the magnetization $S_{\mathrm{Mn}}(i)$ of the Mn spins is increased by the magnetic field, their contribution to the effective magnetic field experienced by holes increases, more than compensating the decrease due to the external field H [see Eq. (3.24)].

Chapter 4

Magnetic Response Functions

4.1 Introduction

The fundamental hypothesis of the linear response theory is that one can write a linear relation between an induced effect and the perturbation causing it. In this thesis we study the magnetic response functions (magnetic susceptibilities) for DMS materials described by the band impurity model (2.1). There are two types of magnetic response functions which will be studied: (a) the transverse dynamical susceptibility, which characterizes the linear response to a small, transversal time-dependent magnetic field, and (b) the static longitudinal susceptibility, which is the magnetic response function to a constant magnetic field applied parallel to the intrinsic magnetization direction. These quantities encode useful information about the magnetic properties of the system: the poles of the dynamical susceptibility give the spin-wave spectrum, whereas the static longitudinal susceptibility is divergent at the critical temperature T_c.

In this chapter we describe the formalism to compute these susceptibilities at zero and at finite temperatures. In the following chapters, we use this formalism to compute the susceptibilities in both ordered and disordered systems.

4.2 Dynamical susceptibility

The most general linear coupling to a time and space dependent external field is described by the interaction term:

$$H_{ext} = \sum_{i\alpha,j\beta} f_{i\alpha,j\beta}(t)\, c^{\dagger}_{i\alpha} c_{j\beta} + \sum_{i} \vec{h}_i(t) \cdot \vec{S}_i \tag{4.1}$$

Some examples are the coupling to external electric fields $\hat{\rho}\phi(t)$ or $\hat{\vec{j}} \cdot \vec{A}(t)$ or magnetic fields $\vec{S} \cdot \vec{B}(t)$. The density of charge $\hat{\rho}$, the density of current $\hat{\vec{j}}$ and the spin $\vec{S}$ operators are all quadratic combinations of electron creation and annihilation operators. For the specific case of magnetic external fields the first term in [4.1] describes the coupling of the carriers to the magnetic field and the second term describes the coupling of the Mn spins to the magnetic field:

$$H_{ext}(t) = -g\mu_B \sum_i \vec{H}(i,t) \cdot \frac{1}{2} c^{\dagger}_{i\alpha} \vec{\sigma}_{\alpha\beta} c_{i\beta} - \tilde{g}\mu_B \sum_i \vec{H}(i,t) \cdot \vec{S}_i \tag{4.2}$$

Throughout this paper we assume that $g = \tilde{g}$. In Ref. [11] it was shown that the specific value of the g-factor for the holes is not important because the magnetic properties of the system are dominated by the Mn spins. Mn spins interact with at most one hole, and the external magnetic field can have a large effect on them. On the other hand, each hole strongly interacts with several Mn spins and the external magnetic field has little direct effect on the holes.

For an interaction with an external magnetic field (4.2), the elements of the general interaction (4.1) are

$$\begin{aligned} \vec{h}_i(t) &= \vec{H}(i,t) \qquad f_{i\sigma,j\sigma}(t) = \delta_{ij} H^z(i,t)\frac{\sigma}{2} \\ f_{i\downarrow,j\uparrow}(t) &= \delta_{ij}\frac{H^+(i,t)}{2} \qquad f_{i\uparrow,j\downarrow}(t) = \delta_{ij}\frac{H^-(i,t)}{2} \end{aligned} \tag{4.3}$$

where the factor $-g\mu_B$ has been absorbed into the units, and $H^{\pm} = H_x \pm iH_y$.

For computing the response functions, it is necessary to find a linear relation between the effect (magnetization) and the perturbation (small magnetic field). This linear relation can be obtained applying many-body perturbation techniques. For zero temperature, the relevant approximation is the Random Phase Approximation, a limiting case of the Time Dependent Hartree-Fock Approximation. For finite temperatures, a generalization based on a variational density matrix approach is used.

4.2.1 The Random Phase Approximation at $T = 0$

We are interested in finding the effects of the perturbation on the ground-state of the system. Since the reference state is the self consistent HF ground-state $|\Psi_0\rangle$ [Eq. (3.21)], it is convenient to work with the one-particle operators which diagonalize this state [Eq. (3.13)]. In terms of these operators, the external interaction becomes:

$$H_{ext} = \lambda \sum_{n\alpha,m\beta} f_{n\alpha,m\beta}(t)\, a^{\dagger}_{n\alpha} a_{m\beta} + \lambda \sum_i \vec{h}_i(t)\cdot\vec{S}_i \tag{4.4}$$

where $f_{n\alpha,m\beta}$ are given by:

$$f_{n\alpha,m\beta}(t) = \sum_{ij} \psi^*_{n\alpha}(i)\psi_{m\beta}(j) f_{i\alpha,j\beta}(t). \tag{4.5}$$

and can be computed once the self-consistent HF ground-state is known. Here λ characterizes the strength of the weak external field ($\lambda << 1$) and is introduced as a device to keep track of the order of perturbation. Using perturbation theory the wave function of the system in the presence of H_{ext} has the general form $|\Psi_0(t)\rangle + \lambda|\Psi_1(t)\rangle + \ldots$, where $|\Psi_0(t)\rangle = e^{-iE_{GS}t/\hbar}|\Psi_0\rangle$ is the HF ground state wave function. The first order perturbation in the wave function induces small (first-order) deviations of the self-consistent fields from their ground-state self consistent values. For example, for an arbitrary observable operator $\hat{A}$:

$$\langle\hat{A}\rangle \rightarrow \langle\hat{A}\rangle + \lambda\,\delta(\hat{A}) + \mathcal{O}(\lambda^2) \tag{4.6}$$

where $\langle \hat{A} \rangle = \langle \Psi_0 | \hat{A} | \Psi_0 \rangle$ is the self consistent mean-field value and:

$$\delta(\hat{A}) = \langle \Psi_0(t) | \hat{A} | \Psi_1(t) \rangle + cc \tag{4.7}$$

In the case of our Hamiltonian (2.1), the expectation values of the operators $\vec{S}_i$ and $\vec{s}_i$ undergo such changes, which modify the mean-field Hamiltonian (3.20). The first order contributions must be included in the total perturbation; as a result, we define the effective interaction Hamiltonian as following:

$$H_{\text{eff}}(t) = H_{ext}(t) + \lambda \sum_{i,j} J_{ij} \left[\delta(\vec{S}_i) \cdot \vec{s}_j + \vec{S}_i \cdot \delta(\vec{s}_j) \right] \tag{4.8}$$

In terms of the HF operators, this becomes:

$$\begin{aligned} H_{\text{eff}}(t) = H_{ext}(t) &+ \lambda \sum_{n,m,i} J_{n\uparrow,m\downarrow}(i) \left[a^\dagger_{n\uparrow} a_{m\downarrow} \, \delta(S_i^-) + \delta(a^\dagger_{n\uparrow} a_{m\downarrow}) \, S_i^- \right] \\ &+ \lambda \sum_{n,m,i} J_{n\downarrow,m\uparrow}(i) \left[a^\dagger_{n\downarrow} a_{m\uparrow} \, \delta(S_i^+) + \delta(a^\dagger_{n\downarrow} a_{m\uparrow}) S_i^+ \right] \\ &+ \lambda \sum_{n,m,\sigma,i} J_{n\sigma,m\sigma}(i) \, \sigma \left[a^\dagger_{n\sigma} a_{m\sigma} \, \delta(S_i^z) + \delta(a^\dagger_{n\sigma} a_{m\sigma}) S_i^z \right] \end{aligned} \tag{4.9}$$

where

$$J_{n\alpha,m\beta}(i) = \frac{1}{2} \sum_j J_{ij} \psi^*_{n\alpha}(j) \psi_{m\beta}(j). \tag{4.10}$$

Throughout this thesis, we use the following index convention: indexes $i, j, \ldots$ run over all Mn sites, $i = 1, \ldots, N_d$ etc. Indexes $p, p', \ldots$ run over all the "particle" occupied spin-down states in the HF ground-state, $p = 1, \ldots, N_h$ etc; indexes $h, h', \ldots$ run over all "hole" empty spin-up states in the HF ground-state, $h = 1, \ldots, N_d$ etc.

Using this effective perturbation, the first order correction $|\Psi_1(t)\rangle$ can be determined by solving the time-dependent Schrödinger equation up to first order in λ, or by doing time dependent perturbation theory in the interaction picture. In either case, we find:

$$\begin{aligned} |\Psi_1(t)\rangle = e^{(-\frac{i}{\hbar} E_{GS} t)} \Bigg(&\sum_{p=1}^{N_h} \sum_{h=1}^{N_d} \int_{-\infty}^{\infty} \frac{d\omega}{2\pi} \frac{x_{hp}(\omega) \exp(-i\omega t)}{\hbar\omega - (E_{h\uparrow} - E_{p\downarrow}) + i\eta} a^+_{h\uparrow} a_{p\downarrow} \\ &+ \sum_{i=1}^{N_d} \int_{-\infty}^{\infty} \frac{d\omega}{2\pi} \frac{y_i(\omega) \exp(-i\omega t)}{\hbar\omega - H_i + i\eta} \frac{S_i^-}{\sqrt{2S}} \Bigg) |\Psi_0\rangle \end{aligned} \tag{4.11}$$

Here $E_{h\uparrow} - E_{p\downarrow}$, respectively H_i, are the mean-field energy costs to flip a charge carrier spin, respectively a Mn spin [see Eqs. (3.1), (3.14)]. The coefficients $x_{hp}(\omega)$ and $y_i(\omega)$ [the Fourier transforms of $x_{hp}(t)$ and $y_i(t)$], are given by

$$x_{hp}(\omega) = f_{h\uparrow,p\downarrow}(\omega) + \sum_i J_{h\uparrow,p\downarrow}(i) \, \delta(S_i^-)(\omega) \tag{4.12}$$

$$y_i(\omega) = \sqrt{2S}\left(\frac{h_i^+(\omega)}{2} + \sum_{n.m} J_{n\uparrow,m\downarrow}(i)\,\delta(a_{n\uparrow}^\dagger a_{m\downarrow})(\omega)\right) \tag{4.13}$$

We then obtain a set of self consistent equations for determining $x_{hp}(\omega)$ and $y_i(\omega)$, by calculating the expectation values $\delta(a_{n\uparrow}^\dagger a_{m\downarrow})(\omega)$ and $\delta(S_i^-)(\omega)$ using the wave function (4.11) and definition (4.7), to find:

$$\begin{aligned}\delta(a_{n\uparrow}^\dagger a_{m\downarrow})(\omega) &= -\sum_{p=1}^{N_h}\sum_{h=1}^{N_d}\frac{\delta_{pm}\delta_{nh}\; x_{hp}^*(-\omega)}{\hbar\omega + (E_{h\uparrow} - E_{p\downarrow}) + i\eta} \\ \delta(S_i^-)(\omega) &= -\sqrt{2S}\frac{y_i^*(-\omega)}{\hbar\omega + H_i + i\eta}\end{aligned} \tag{4.14}$$

By inserting Eqs. (4.14) into Eqs. (4.12) and (4.13), we get the self consistent equations:

$$\begin{aligned}x_{hp}^*(-\omega) &= f_{h\uparrow p\downarrow}^*(-\omega) + \sum_i J_{h\uparrow p\downarrow}^*(i)\frac{\sqrt{2S}y_i(\omega)}{\hbar\omega - H_i + i\eta} \\ y_i(\omega) &= \frac{\sqrt{2S}}{2}h_i^+(\omega) - \sqrt{2S}\sum_{p=1}^{N_h}\sum_{h=1}^{N_d} J_{h\uparrow p\downarrow}(i)\frac{x_{hp}^*(-\omega)}{\hbar\omega + (E_{h\uparrow} - E_{p\downarrow}) + i\eta}\end{aligned} \tag{4.15}$$

These two equation can be reformulated in a more familiar form by defining a new set of unknowns $X_{hp}(\omega)$ and $Y_i(\omega)$:

$$\begin{aligned}X_{hp}(\omega) &= \frac{x_{hp}^*(-\omega)}{\hbar\omega + (E_{h\uparrow} - E_{p\downarrow}) + i\eta} \\ Y_i(\omega) &= \frac{y_i(\omega)}{\hbar\omega - H_i + i\eta},\end{aligned} \tag{4.16}$$

It should be noticed, by direct comparison with Eq. (4.14), that the new variables are just $X_{hp}(\omega) = -\delta(a_{h\uparrow}^\dagger a_{p\downarrow})(\omega)$ and $Y_i(\omega) = \sqrt{2S}\delta(S_i^+)(\omega)$. In terms of these variables, the self-consistency conditions Eq. (4.15), become:

$$[\hbar\omega + E_{h\uparrow} - E_{p\downarrow}]\,X_{hp}(\omega) = \sqrt{2S}\sum_i J_{p\downarrow,h\uparrow}(i)Y_i(\omega) + f_{p\downarrow,h\uparrow}(\omega) \tag{4.17}$$

$$[\hbar\omega - H_i]\,Y_i(\omega) = -\sqrt{2S}\sum_{p=1}^{N_h}\sum_{h=1}^{N_d} J_{p\downarrow,h\uparrow}^*(i)X_{hp}(\omega) + \frac{\sqrt{2S}}{2}\,h_i^+(\omega) \tag{4.18}$$

These equations can be recast in the standard RPA form:

$$\hbar\omega\begin{pmatrix}\mathbf{X}\\ -\mathbf{Y}\end{pmatrix} = \begin{pmatrix}\mathbf{E} & \mathbf{J}\\ \mathbf{J}^* & \mathbf{H}\end{pmatrix}\cdot\begin{pmatrix}\mathbf{X}\\ \mathbf{Y}\end{pmatrix} + \begin{pmatrix}\mathbf{f}\\ \mathbf{h}\end{pmatrix} \tag{4.19}$$

The vectors $\mathbf{X}$ and $\mathbf{Y}$ contain the unknowns X_{hp} and Y_i . Matrices $\mathbf{E}$, $\mathbf{H}$, $\mathbf{J}$ have the elements $\mathbf{E}_{hp,h'p'} = -\delta_{hh'}\delta_{pp'}(E_{h\uparrow} - E_{p\downarrow})$, $\mathbf{H}_{i,i'} = -\delta_{i,i'}H_i$, $\mathbf{J}_{hp,i} = \sqrt{2S}J_{p\downarrow,h\uparrow}(i)$ while $\mathbf{f}$ and $\mathbf{h}$ contain the external fields $f_{h\uparrow,p\downarrow}(\omega)$ and $\frac{\sqrt{2S}}{2}h_i^+(\omega)$.

In the absence of the external fields, this is an eigenequation whose eigenvalues $\hbar\omega$ are the energies of the collective spin-wave modes, as well as the continuum of particle-hole spin-flipping excitations (see Ref. [15]). The dimension of the RPA matrix is $N_d + N_h \times N_d$. Of these solutions N_d are proper spin collective mode and $N_h \times N_d$ are particle-hole spin-flip continuum modes.

Because we have more Mn spins than charge carriers and because Mn have larger spins than the charge carriers, the dominant change in the magnetization of the system comes from changes in the Mn spins polarization, described by the $Y_i = \sqrt{2S}\delta(S_i^+)(\omega)$ coefficients. We can find these by solving for the X_{hp} coefficients from equation (4.17) and inserting the solutions into equation (4.18) to obtain a system of N_d inhomogeneous linear equations:

$$\sum_j M_{ij}(\omega)\ \delta(S_j^+)(\omega) = B_i(\omega) \tag{4.20}$$

where

$$M_{ij}(\omega) = \delta_{ij}(\hbar\omega - H_i) + 2S \sum_{p=1}^{N_h} \sum_{h=1}^{N_d} \frac{J^*_{p\downarrow,h\uparrow}(i) J_{p\downarrow,h\uparrow}(j)}{\hbar\omega + E_{h\uparrow} - E_{p\downarrow} + i\eta} \tag{4.21}$$

$$B_i(\omega) = S\, h_i^+(\omega) - 2S \sum_{p=1}^{N_h} \sum_{h=1}^{N_d} \frac{J^*_{p\downarrow,h\uparrow}(i) f_{p\downarrow,h\uparrow}(\omega)}{\hbar\omega + E_{h\uparrow} - E_{p\downarrow} + i\eta} \tag{4.22}$$

In this method, for each ω of interest we calculate the matrix $\mathbf{M}(\omega)$ and the vector $\mathbf{B}(\omega)$, using HF ground-state known quantities. This allows us to find all $\delta(S_i^+)(\omega)$ expectation values. This method is much more efficient than directly solving the RPA matrix equation because we are dealing with much smaller matrices and therefore we can go to sizes as large as $N_d \approx 500$. If need be, the coefficients X_{hp} characterizing the variations in the charge carrier spin expectation values can then also be computed, from Eq. (4.17). This approach has been justified in reference [15] for obtaining the spin-wave spectrum.

Up to now the general form of an external interaction (4.1) has been used; restriction to the case of an external magnetic field [Eq. (4.3)] implies that:

$$f_{p\downarrow,h\uparrow}(\omega) = \frac{1}{2} \sum_i H^+(i,\omega) \psi^*_{p\downarrow}(i) \psi_{h\uparrow}(i); \qquad h_i^+(\omega) = H^+(i,\omega) \tag{4.23}$$

One important point to notice here is that each of the $B_i(\omega)$ source terms is a linear combination of $H^+(i,\omega)$, $i = 1, ..., N_d$. Also, our variables in equation (4.20) are $\delta(S_i^+)(\omega)$ which imply that what we find in this approximation is a response function to a rotating transversal magnetic field, in other words a transversal dynamical susceptibility.

The other aspect of this approximation is that even though we started with an external magnetic field with an arbitrary direction we find no changes of the magnetization in the longitudinal direction, $\delta(S_i^z)(\omega) = 0$ if $\omega \neq 0$. This is due to the fact that for any periodic variations of the magnetic field, the

induced magnetization along any fixed direction averages to zero over a long time interval. This argument also holds for finite temperatures.

We can now define the transversal dynamical susceptibility as

$$\delta(S_{\vec{q}}^{+})(\omega) = \chi(\vec{q},\omega)H^{+}(\vec{q},\omega)$$

where $H^{+}(i,\omega) = e^{i\vec{q}\cdot\vec{R}_i}H^{+}(\omega)$ and $\delta(S_{\vec{q}}^{+})(\omega) = \frac{1}{N_d}\sum_i e^{-i\vec{q}\cdot\vec{R}_i}\delta(S_i^{+})(\omega)$. Since the inhomogeneous terms in Eq. (4.20) are all proportional to $H^{+}(\omega)$, we can set $H^{+}(\omega) = 1$, solve for $\delta(S_i^{+})(\omega)$ and use

$$\chi(\vec{q},\omega) = \frac{4xg^2\mu_b^2}{a^3}\frac{1}{N_d}\sum_i e^{-i\vec{q}\cdot\vec{R}_i}\delta(S_i^{+})(\omega) \tag{4.24}$$

The multiplying factor in the front has the role of establishing the correct units. For the dynamical susceptibility, all the samples we consider have the same concentration $x = 0.01$. Therefore we will set the proportionality factor to unity and express the susceptibility in units of $4x(g\mu_b)^2/a^3$. In disordered systems, expression (4.24) implies an average over many disorder realizations, so that invariance to proper lattice translations is regained.

4.2.2 The Random Phase Approximation at Finite T

In this section we generalize the formalism of the last section to finite temperatures. At finite T, the system is not in a pure state and therefore an approximation based on a density matrix should be used. To realize this two different steps must be taken: first the variational action of the system should be minimized to derive the equations of motion. Secondly, we apply perturbational methods to find the dynamical response function to the small external perturbation.

Here again we consider the external interaction in the form of Eq. (4.4). The full Hamiltonian is, then:

$$\mathcal{H}(t) = \sum_{i,j,\sigma} t_{ij}c_{i\sigma}^{\dagger}c_{j\sigma} + \sum_{i,j} J_{ij}\vec{S}_i\cdot(c_{j\alpha}^{\dagger}\frac{\vec{\sigma}_{\alpha\beta}}{2}c_{j\beta})$$

$$+\lambda e^{\eta t}\Big(\sum_{i\alpha j\beta} f_{i\alpha,j\beta}(t)\,c_{i\alpha}^{+}c_{j\beta} + \sum_i \vec{h}_i(t)\cdot\vec{S}_i\Big), \tag{4.25}$$

where the factor λ is used to keep track of the perturbation order and the factor $e^{\eta t}$ is used to adiabatically turn on the perturbation at $t = -\infty$.

The variational principle for the time evolution of a system described by a density operator requires the minimization of the functional [22]:

$$S_{\mathcal{H}} = -\int_{t_i}^{t_f} dt\, Tr\left\{\mathcal{A}\hbar\frac{d\mathcal{D}}{dt} + i\mathcal{A}[\mathcal{H},\mathcal{D}]\right\} + Tr\mathcal{D}(t_f)\mathcal{A}(t_f), \tag{4.26}$$

where $\mathcal{H}$ is the time dependent Hamiltonian and $S_{\mathcal{H}}$ is a functional of the time dependent operators $\mathcal{A}(t)$ and $\mathcal{D}(t)$. Here, $\mathcal{D}(t)$ represents a variational

density matrix operator of the system and $\mathcal{A}(t)$ any operator associated with some observable. The equations of motion for $\mathcal{A}(t)$ and $\mathcal{D}(t)$ are obtained by requiring that $S_{\mathcal{H}}$ be stationary with respect to all possible variations of $\mathcal{A}(t)$ and $\mathcal{D}(t)$ subject to the conditions

$$\mathcal{D}(t_i) = \mathcal{D}_i, \qquad \mathcal{A}(t_f) = \mathcal{A}_i. \tag{4.27}$$

where $\mathcal{A}_i$ and $\mathcal{D}_i$ are two fixed operators.

The variational approximation is obtained by restricting ourselves to a certain class of operators $\mathcal{A}(t)$ and $\mathcal{D}(t)$ which allow for the explicit calculation of $S_{\mathcal{H}}$. The density matrix $\hat{\mathcal{D}}(t)$ is taken to be of the form

$$\hat{\mathcal{D}}(t) = \frac{e^{-\beta(\hat{\mathcal{K}}-\mu\hat{\mathcal{N}})}}{\mathcal{Z}}. \tag{4.28}$$

where the variational Hamiltonian $\hat{\mathcal{K}}(t)$ is chosen to be

$$\hat{\mathcal{K}}(t) = \sum_{ij,\alpha\beta} h_{i\alpha,j\beta}(t)\, c^{\dagger}_{i\alpha} c_{j\beta} - \sum_i \vec{H}_i(t) \cdot \vec{S}_i. \tag{4.29}$$

The operator $\hat{\mathcal{A}}$ is taken to be of similar form as $\hat{\mathcal{K}}$, *i.e.*:

$$\hat{\mathcal{A}}(t) = \sum_{\substack{i,j \\ \alpha\beta}} a_{i\alpha,j\beta}(t) c^{\dagger}_{i\alpha} c_{j\beta} - \sum_i \vec{A}_i(t) \cdot \vec{S}_i. \tag{4.30}$$

The boundary condition (4.27) for the density matrix $\hat{\mathcal{D}}$ at the initial time $t_i = -\infty$ is taken as

$$\hat{\mathcal{D}}(-\infty) = \hat{\mathcal{D}}_0 \tag{4.31}$$

where $\hat{\mathcal{D}}_0$ is the Hartree Fock density matrix (3.3). The reason for this boundary condition is that at $t_i = -\infty$, the interaction with the external magnetic field vanishes due to the adiabatic factor $e^{\eta t}$, and therefore the system is considered to be well described within the static mean-field scheme.

With these definitions for the class of variational operators $\hat{\mathcal{A}}(t)$ and $\hat{\mathcal{D}}(t)$, we are now able to express the variation of the functional $S_{\mathcal{H}}$ in terms of $\hat{\mathcal{D}}(t)$ and $\hat{\mathcal{K}}(t)$ matrix elements. Similar to the derivation for the static mean-field approximation, we define the following two expectation values

$$\rho_{i\alpha,j\beta}(t) = Tr[\hat{\mathcal{D}}\, c^{\dagger}_{j\beta} c_{i\alpha}]$$

$$\vec{S}(i,t) = Tr[\hat{\mathcal{D}}\vec{S}_i]. \tag{4.32}$$

The functional $S_{\mathcal{H}}$ can be expressed in terms of these expectation values:

$$S_{\mathcal{H}} \;=\; -\hbar \int_{t_i}^{t_f} dt \sum_{\substack{i,j \\ \alpha\beta}} a_{i\alpha,j\beta}(t) \frac{d}{dt} \rho_{j\beta,i\alpha}(t) - \sum_i \vec{A}_i(t) \cdot \frac{d}{dt} S(\vec{i},t)$$

$$-i\int_{t_i}^{t_f} dt \sum_{\substack{i,j\\ \alpha\beta}} \sum_{k\lambda} H_{i\alpha j\beta}\Big(\rho_{j\beta,k\lambda}(t)a_{k\lambda,i\alpha}(t) - a_{j\beta,k\lambda}(t)\rho_{k\lambda,i\alpha}(t)\Big)$$
$$-\int_{t_i}^{t_f} dt \sum_{\substack{i,j\\ \alpha\beta}} \vec{S}(i,t)\cdot\vec{A}_i(t)\times\Big(J_{ij}\frac{\vec{\sigma}_{\alpha\beta}}{2}\rho_{j\beta,j\alpha}(t) + \lambda e^{\eta t}\delta_{\alpha\beta}\delta_{ij}\vec{h}_i(t)\Big)$$
$$+\sum_{\substack{i,j\\ \alpha\beta}} a_{i\alpha,j\beta}(t_f)\rho_{j\beta,i\alpha}(t_f) - \sum_i \vec{A}_i(t_f)\cdot\vec{S}(i,t_f) \tag{4.33}$$

where $H_{i\alpha,j\beta}(t)$ are defined by

$$H_{i\alpha,j\beta}(t) = t_{ij}\delta_{\alpha\beta} + \lambda e^{-\eta t} f_{i\alpha,j\beta}(t) + \delta_{ij}\sum_m J_{mi}\frac{\vec{\sigma}_{\alpha\beta}}{2}\cdot\vec{S}(m,t). \tag{4.34}$$

We now calculate the variation of the functional $S_{\mathcal{H}}$ due to variations of the matrix elements of the operators $\mathcal{A}$ and $\mathcal{D}$. After a lengthy but straightforward calculation, we find:

$$\begin{aligned}\delta S_{\mathcal{H}} \;=\; & \int_{t_i}^{t_f} dt\Big\{\sum_{\substack{i,j\\ \alpha\beta}} \delta a_{i\alpha,j\beta}(t)\; T^{(1)}_{i\alpha,j\beta}(t) + \sum_i \delta\vec{A}_i(t)\cdot\vec{T}^{(2)}_i \\ & + \sum \delta\rho_{j\beta,i\alpha}(t)\, T^{(3)}_{i\alpha,j\beta} + \sum_i \delta\vec{S}(i,t)\cdot\vec{T}^{(4)}_i\Big\} = 0\end{aligned} \tag{4.35}$$

where the expressions T^1, T^2, T^3, T^4 will be presented momentarily. The four equations of motion (EOM), obtained from requesting that $\delta S_{\mathcal{H}} = 0$, are then:

$$\begin{aligned} T^{(1)}_{i\alpha,j\beta}(t) &= 0 \qquad \vec{T}^{(2)}_i = 0 \\ T^{(3)}_{i\alpha,j\beta}(t) &= 0 \qquad \vec{T}^{(4)}_i = 0 \end{aligned} \tag{4.36}$$

The first equation, $T^{(1)}_{i\alpha,j\beta}(t) = 0$ reads

$$i\hbar\frac{d}{dt}\rho_{j\beta,i\alpha}(t) = \sum_{k\lambda}\left[H_{j\beta,k\lambda}(t)\rho_{k\lambda,i\alpha}(t) - \rho_{j\beta,k\lambda}(t)H_{k\lambda,i\alpha}(t)\right] \tag{4.37}$$

while the second equation, $\vec{T}^{(2)}_i = 0$, can be expressed as

$$\frac{d}{dt}\vec{S}(i,t) = \vec{h}_{\text{eff}}(i,t)\times\vec{S}(i,t) \tag{4.38}$$

where

$$\vec{h}_{\text{eff}}(i,t) = \sum_{j\beta\alpha} J_{ij}\frac{\vec{\sigma}_{\alpha\beta}}{2}\rho_{j\beta,j\alpha}(t) + \lambda e^{\eta t}\vec{h}_i(t). \tag{4.39}$$

Equation (4.37) is the simply the Heisenberg equation $i\hbar d\rho/dt = [H,\rho]$ for the expectation value of the operator $c^\dagger_{j\beta}c_{i\alpha}$, since $H_{j\beta,k\lambda}(t)$ is the matrix element of the effective fermionic Hamiltonian [Eq. (4.34)]. The second equation describes the time evolution of the Mn spin in an effective magnetic field

$\vec{h}_{\rm eff}(i,t)$. The two other equations obtained from requesting that $\delta S_{\mathcal{H}} = 0$ give the equations of motion for $a_{i\alpha,j\beta}(t)$ and $\vec{A}_i(t)$ defining the evolution of the operator $\mathcal{A}$, which allow one to find its time-dependent expectation value. Since we are only interested in the expectation value of the Mn spins, given by Eq. (4.38), we do not need to use these supplementary equations.

Equations (4.37) and (4.38) give the general time-dependence of those expectation values, for any value of the external coupling. However, we are interested in the linear regime where the external field is perturbationally small, and the expectation values are close to the self-consistent static solutions. The boundary condition $\hat{\mathcal{D}}(-\infty) = \hat{\mathcal{D}}_0$ implies that

$$\rho_{j\beta,i\alpha}(-\infty) = \delta_{\alpha\beta}\,\rho_{ji,\alpha}$$
$$\vec{S}(i,-\infty) = \vec{e}_z\, S_{\rm Mn}(i). \tag{4.40}$$

where $\rho_{ji,\alpha}$ and $S_{\rm Mn}(i)$ are the self-consistent static mean-field solutions at the same temperature T [Eqs. (3.5), (3.6)]. As the interaction is adiabatically turned on, to first order in perturbation theory we expect that these expectation values become of the general form:

$$\rho_{j\beta,i\alpha}(t) = \delta_{\alpha\beta}\,\rho_{ji,\alpha} + \lambda e^{\eta t}\,\delta\rho_{j\beta,i\alpha}(t) + \mathcal{O}(\lambda^2)$$
$$\vec{S}(i,t) = \vec{e}_z S_{\rm Mn}(i) + \lambda e^{\eta t}\,\delta\vec{S}(i,t) + \mathcal{O}(\lambda^2). \tag{4.41}$$

To first order in λ, the effective Hamiltonian (4.34) defining the dynamics of the charge carrier operators, respectively the effective magnetic field (4.39) defining the spin dynamics become:

$$H_{i\alpha,j\beta}(t) = \delta_{\alpha\beta}h_{ij,\alpha} + \lambda e^{\eta t}\,H^{(1)}_{i\alpha,j\beta}(t) + \mathcal{O}(\lambda^2) \tag{4.42}$$

$$\vec{h}_{\rm eff}(i) = \sum_{j\alpha} J_{ij}\frac{\alpha}{2}\,\rho_{jj,\alpha}\vec{e}_z + \lambda e^{\eta t}\,\vec{h}^{(1)}_{\rm eff}(i,t) + \mathcal{O}(\lambda^2). \tag{4.43}$$

where

$$H^{(1)}_{i\alpha,j\beta}(t) = f_{i\alpha,j\beta}(t) + \delta_{i,j}\sum_m J_{mi}\frac{\vec{\sigma}_{\alpha\beta}}{2}\delta\vec{S}(m,t),$$

$$\vec{h}^{(1)}_{\rm eff}(i,t) = \sum_{j\beta\alpha} J_{ij}\frac{\vec{\sigma}_{\alpha\beta}}{2}\delta\rho_{j\beta,j\alpha}(t) + \vec{h}_i(t)$$

The first terms in Eq. (4.42) and Eq. (4.43) are just the static mean-field Hamiltonian $h_{ij,\alpha}$ [Eq. (3.12)], respectively the static mean-field effective magnetic field H_i [Eq. (3.11)], as expected.

We now substitute these expressions into Eqs. (4.37) and (4.38). The zero order terms recover the expected static mean-field solution, whereas the first-order contributions give the following equations:

$$\begin{aligned} i\hbar\frac{d}{dt}[e^{\eta t}\,\delta\rho_{j\beta,i\alpha}(t)] &= e^{\eta t}\sum_k [h_{jk,\beta}\delta\rho_{k\beta,i\alpha}(t) - h_{ki,\alpha}\,\delta\rho_{j\beta,k\alpha}(t)] \\ &\quad + e^{\eta t}\sum_k [H^{(1)}_{j\beta,k\alpha}(t)\rho_{ki,\alpha} - H^{(1)}_{k\beta,i\alpha}(t)\rho_{ik,\beta}], \end{aligned} \tag{4.44}$$

$$\frac{d}{dt}[e^{\eta t}\,\delta\vec{S}(i,t)] = e^{\eta t}\big\{ - H_i\,\vec{e_z}\times\delta\vec{S}(i,t) + \vec{h}^{(1)}_{\rm eff}(i,t)\times\vec{e_z}S_{\rm Mn}(i)\big\}. \qquad (4.45)$$

These equations are in fact the RPA equations analogous to Eqs. (4.17) and (4.18). To demonstrated this we first Fourier transform them:

$$\begin{aligned}(\hbar\omega + i\eta)\,\delta\rho_{j\beta,i\alpha}(\omega) &= \sum_k [h_{jk,\beta}\delta\rho_{k\beta,i\alpha}(\omega) - h_{ki,\alpha}\delta\rho_{j\beta,k\alpha}(\omega)] \\ &\quad + \sum_k [H^{(1)}_{j\beta k\alpha}(\omega)\rho_{ki,\alpha} - H^{(1)}_{k\beta i\alpha}(\omega)\rho_{ik,\beta}], \qquad (4.46)\end{aligned}$$

(From now on we redefine the $\hbar\eta \to \eta$ such that η has energy units).

Equation (4.45) contains 3 different equations for the components $\delta S_r(i,t)$, where $r = x, y, z$. The equations for the x and y components can be grouped together by defining $\delta S_+(i,t) = \delta S^x(i,t) + i\delta S^y(i,t)$. After a Fourier transformation, the resulting equations are:

$$(\hbar\omega + i\eta)\delta S_z(i,\omega) = 0,$$

$$(\hbar\omega - H_i + i\eta)\,\delta S_+(i,\omega) = \sum_j J_{ij}\delta\rho_{j\downarrow,j\uparrow}(t)S_{\rm Mn}(i) + h_i^+(\omega)S_{\rm Mn}(i). \qquad (4.47)$$

The first equation shows that for $\omega \neq 0$, we have $\delta S_z(i,\omega) = 0$ which indicates that $S_{\rm Mn}(i)$ is conserved. This means that the mean-field fermionic Hamiltonian (3.12) and therefore the mean field energy levels $E_{n\sigma}$, are all unchanged to first order in the perturbation. This implies that for $\omega \neq 0$ the chemical potential μ is also unchanged (to first order) from its static mean-field value. This can also be seen from the fact that from Eq. (4.46) it follows that $(\hbar\omega + i\eta)\sum_{i,\alpha}\delta\rho_{i\alpha,i\alpha} = 0$ which means that to first order,

$$\sum_{i,\alpha}\rho_{i\alpha,i\alpha}(\omega) = \sum_{i,\alpha}\left[\rho_{ii,\alpha} + \lambda e^{\eta t}\delta\rho_{i\alpha,i\alpha}(\omega)\right] = \sum_{i,\alpha}\rho_{ii,\alpha} = N_h$$

Thus far we have demonstrated that the mean-field Hamiltonian, energy levels and therefore the occupation numbers $f(E_{n\sigma})$ maintain their static mean-field values up to first order in the perturbation. We can therefore use the results from the static Hartree-Fock section to simplify Eqs. (4.46) and (4.47). This, however, is only true for a time-dependent external field, $\omega \neq 0$. For a static external field $\omega \to 0$ and we cannot conclude anymore that $\delta S_z(i,\omega)$ and $\sum_{i,\alpha}\delta\rho_{i\alpha,i\alpha}(\omega)$ are zero. In fact, as we will demonstrate in the next section, these quantities are not zero in the static case.

We can now proceed to diagonalize the RPA equations (4.46) and (4.47). We start by defining:

$$X_{nm}(\omega) = \sum_{ij}\psi_{n\uparrow}(i)\psi^*_{m\downarrow}(j)\delta\rho_{j\downarrow,i\uparrow}(\omega) \qquad (4.48)$$

$$\widetilde{f}_{nm}(\omega) = [f(E_{n\uparrow}) - f(E_{m\downarrow})]\sum_{ij}\psi_{n\uparrow}(i)\psi^*_{m\downarrow}(j)f_{j\downarrow,i\uparrow}(\omega), \qquad (4.49)$$

Eq. (4.46) can be rewritten as:

$$\begin{aligned}(\hbar\omega + i\eta)\delta\rho_{j\downarrow,i\uparrow}(\omega) &= \sum_k [h_{jk,\downarrow}\,\delta\rho_{k\downarrow,i\uparrow}(\omega) - h_{ki,\uparrow}\,\delta\rho_{j\downarrow,k\uparrow}(\omega)] \\ &\quad + \sum_k [\rho_{ki,\uparrow}\,f_{j\downarrow k\uparrow}(\omega) - \rho_{jk,\downarrow}\,f_{k\downarrow i\uparrow}(\omega)] \\ &\quad + \frac{1}{2}\sum_k [J_{jk}\,\rho_{ji,\uparrow} - J_{ik}\rho_{ji,\downarrow}]\,\delta S_+(k,\omega) \qquad (4.50)\end{aligned}$$

¿From this we can derive an equation for $X_{nm}(\omega)$ [Eq. (4.48)], which, after we make use of the static Hartree-Fock equations for $\rho_{ki,\alpha}$ and $h_{jk,\beta}$ [Eqs. (3.15), (3.16)], and use notation (4.49), becomes:

$$[\hbar\omega + E_{h\uparrow} - E_{p\downarrow} + i\eta]X_{hp}(\omega) = \widetilde{f}_{hp}(\omega) + [f(E_{h\uparrow}) - f(E_{p\downarrow})]\sum_j J_{p\downarrow,h\uparrow}(j)\delta S_+(j,\omega) \qquad (4.51)$$

while Eq. (4.47) can be rewritten as:

$$(\hbar\omega - H_i + i\eta)\,\delta S_+(i,\omega) = \sum_{p=1}^{N_d}\sum_{h=1}^{N_d} J^*_{p\downarrow,h\uparrow}(i)X_{hp}(\omega) + h_i^+(\omega)S_{\mathrm{Mn}}(i). \qquad (4.52)$$

Equations (4.51) and (4.52) are *the generalized RPA equations*, i.e. the finite temperature generalization of the $T = 0$ RPA equations (4.17) and (4.18). However, unlike in the $T = 0$ case, there are now $N_d + N_d^2$ equations, because all the levels $(p\downarrow)$ are occupied with some probability $f(E_{p\downarrow})$ in the ground-state (at $T = 0$, only the lowest N_h levels are filled while the rest are empty). Similar to our approach in the $T = 0$ case, the values for $X_{\alpha\beta}$ can be found from the first equation (4.51) and substituted into the second equation (4.52), giving a system of N_d linear equations [analogous to (4.20)]:

$$\sum_j M_{ij}(\omega)\delta S_+(j,\omega) = B_i(\omega) \qquad (4.53)$$

where

$$\begin{aligned}M_{ij}(\omega) &= \delta_{ij}(\hbar\omega - H_i + i\eta) - 2S_{\mathrm{Mn}}(i) \\ &\quad \times \sum_{\alpha=1}^{N_d}\sum_{\beta=1}^{N_d} \frac{J^*_{\beta\downarrow,\alpha\uparrow}(i)J_{\beta\downarrow,\alpha\uparrow}(j)}{\hbar\omega + E_{\alpha\uparrow} - E_{\beta\downarrow} + i\eta}[f(E_{\alpha\uparrow}) - f(E_{\beta\downarrow})] \qquad (4.54)\end{aligned}$$

$$B_i(\omega) = S_{\mathrm{Mn}}(i)h_i^+(\omega) + 2S_{\mathrm{Mn}}(i)\sum_{\alpha=1}^{N_d}\sum_{\beta=1}^{N_d}\frac{J^*_{\beta\downarrow,\alpha\uparrow}(i)\widetilde{f}_{\alpha\beta}(\omega)}{\hbar\omega + E_{\alpha\uparrow} - E_{\beta\downarrow} + i\eta} \qquad (4.55)$$

The matrix elements $M_{ij}(\omega)$ and $B_i(\omega)$ can be calculated for each ω value, for any finite temperature. We can then solve for $\delta S_+(j,\omega)$ at each site j and use these values to find the finite-temperature transversal dynamical susceptibility in a manner similar to that described by Eq. (4.24).

4.3 Static Magnetic Susceptibility

In this section we consider the static magnetic susceptibility describing the linear response to a a uniform dc external magnetic field. The transversal static susceptibility is divergent for $T < T_c$, since a transversal magnetic field reorients the direction of the bulk magnetization, leading to a finite change in magnetization irrespective how small the applied magnetic field is. As a result, here we will discuss only the longitudinal static magnetic susceptibility.

As discussed in the last section, application of a $\omega = 0$ static external magnetic field is expected to modify the static mean-field equations to first order. These corrections can be found perturbatively starting from the self-consistent equations in the presence of the magnetic field H, Eqs. (3.11) and (3.12). Similar to the first chapter, we use the upper index H to refer to solutions in the presence of the external field. For convenience, we define the magnetic susceptibility of Mn spins and holes at each site as

$$\chi_{\rm Mn}(i) = \left.\frac{dS^H_{\rm Mn}(i)}{dH}\right|_{H=0} \qquad \chi_h(i) = \left.\frac{ds^H_h(i)}{dH}\right|_{H=0},$$

Our aim is to express these susceptibilities only in the terms of mean-field values of the unperturbed system (i.e., without an external magnetic field). As before, we continue to take $\tilde{g} = g$ and set $g\mu_B = 1$ for simplicity.

For the effective magnetic field of Eq. (3.23), the expectation value of the Mn spin is:

$$S^H_{\rm Mn}(i) = B_S(\beta[H - \sum_j J_{ij}\, s^H_h(j)]), \tag{4.56}$$

where $B_S(x)$ is the Brillouin function for $S = \frac{5}{2}$. It then follows that

$$\chi_{\rm Mn}(i) = \beta\,[1 - \sum_j J_{ij}\,\chi_h(j)]B_S{}'(\beta H_i) \tag{4.57}$$

where $B_S{}'(x) = dB_S(x)/dx = \frac{1}{4}csch^2(\frac{x}{2}) - (S+\frac{1}{2})^2 csch^2[(S+\frac{1}{2})x]$. The next step is to derive the dependence of $\chi_h(i)$ on $\chi_{\rm Mn}(i)$. To first order in H, we have

$$S^H_{\rm Mn}(i) = S_{\rm Mn}(i) + \chi_{\rm Mn}(i)H + \mathcal{O}(H^2).$$

As a result, to first order, the charge-carrier Hamiltonian [see Eq. (3.22)], becomes:

$$h^H_{ij,\sigma} = h_{ij,\sigma} + \delta_{ij}\frac{\sigma}{2}[\sum_j J_{ij}\chi_{\rm Mn}(j) - 1]H + \mathcal{O}(H^2) \tag{4.58}$$

and the perturbation of the mean-field Hamiltonian is

$$H\cdot\mathcal{H}_p = H\sum_{i,\sigma}\frac{\sigma}{2}[\sum_j J_{ij}\chi_{\rm Mn}(j) - 1]c^+_{i\sigma}c_{i\sigma}$$

We now use perturbation theory to find the energies $E^H_{n\sigma}$ and eigenfunctions $\psi^H_{n\sigma}(i)$ to first order. Here we restrict this calculation to the case of a disordered system where all degeneracies are lifted (the ordered case is considered in the next chapter). In this case, we have:

$$\begin{aligned} E^H_{n\sigma} &= E_{n\sigma} + E^{(1)}_{n\sigma} H + \mathcal{O}(H^2) \\ \psi^H_{n\sigma}(i) &= \psi_{n\sigma}(i) + \psi^{(1)}_{n\sigma}(i) H + \mathcal{O}(H^2) \end{aligned} \tag{4.59}$$

where

$$E^{(1)}_{n\sigma} = \langle \psi_{n\sigma} | \mathcal{H}_p | \psi_{n\sigma} \rangle = \sigma \sum_j J_{n\sigma,n\sigma}(j) \chi_{\rm Mn}(j) - \frac{\sigma}{2} \tag{4.60}$$

$$\psi^{(1)}_{n\sigma}(i) = \sum_{k \neq n} \frac{\langle \psi_{k\sigma} | \mathcal{H}_p | \psi_{n\sigma} \rangle}{E_{n\sigma} - E_{k\sigma}} \psi_{k\sigma}(i) = \sigma \sum_{k \neq n;j} \frac{J_{k\sigma,n\sigma}(j) \chi_{\rm Mn}(j)}{E_{n\sigma} - E_{k\sigma}} \psi_{k\sigma}(i) \tag{4.61}$$

where $J_{n\alpha,m\beta}(i)$ is defined in Eq. (4.10). The last necessary step is to compute the variation of the chemical potential $\mu(H)$, to first order in H. We take derivatives with respect to H (and set $H = 0$) from the constraint on the number of particles, $\sum_{n\sigma} f(E^H_{n\sigma}) = N_h$, to obtain:

$$\left. \frac{d\mu(H)}{dH} \right|_{H=0} = \frac{\sum_{n\sigma} E^{(1)}_{n\sigma} g(E_{n\sigma})}{\sum_{n\sigma} g(E_{n\sigma})} \tag{4.62}$$

where

$$g(E) = \frac{1}{\beta} \frac{df(E)}{dE} = -\frac{1}{4} sech^2 \left[\frac{\beta(E-\mu)}{2} \right].$$

The hole susceptibility $\chi_h(i)$ can now be derived by taking the derivative with H of the finite H charge-carrier expectation value:

$$s^H_h(i) = \frac{1}{2} \sum_{n\sigma} \sigma \, |\psi^H_{n\sigma}(i)|^2 f(E^H_{n\sigma}).$$

Setting $H = 0$, we find:

$$\chi_h(i) = \sum_{n\sigma} \frac{\sigma}{2} \left\{ \left[\psi^{(1)}_{n\sigma}(i) \psi^*_{n\sigma}(i) + cc \right] f(E_{n\sigma}) + |\psi_{n\sigma}(i)|^2 \beta \left(E^{(1)}_{n\sigma} - \frac{d\mu}{dH} \right) g(E_{n\sigma}) \right\}. \tag{4.63}$$

Finally, we substitute the expressions for $E^{(1)}_{n\sigma}$, $\psi^{(1)}_{n\sigma}(i)$ and $\frac{d\mu(H)}{dH}|_{H=0}$ from Eqs. (4.60),(4.61) and (4.62) to obtain:

$$\chi_h(i) = \sum_j A_{ij} \chi_{\rm Mn}(j) + B_i \tag{4.64}$$

where

$$\begin{aligned} A_{ij} = \frac{1}{2} \sum_{n\sigma} \sum_{k \neq n} f(E_{n\sigma}) \left\{ \frac{J_{k\sigma,n\sigma}(j) \psi^*_{n\sigma}(i) \psi_{k\sigma}(i) + cc}{E_{k\sigma} - E_{n\sigma}} \right\} + \\ \frac{\beta}{2} \sum_{n\sigma} |\psi_{n\sigma}(i)|^2 g(E_{n\sigma}) \left\{ J_{n\sigma,n\sigma}(j) - \sigma \frac{\sum_{m\alpha} \alpha \, J_{m\alpha,m\alpha}(j) g(E_{m\alpha})}{\sum_{m\alpha} g(E_{m\alpha})} \right\}, \end{aligned} \tag{4.65}$$

and

$$B_i = \frac{\beta}{4}\sum_{n\sigma}|\psi_{n\sigma}(i)|^2 g(E_{n\sigma})\left[\sigma\frac{\sum_{m\alpha}\alpha\, g(E_{m\alpha})}{\sum_{m\alpha} g(E_{m\alpha})} - 1\right]. \tag{4.66}$$

Here it is worth mentioning that in Eq (4.64), the dominant term is $\sum_j A_{ij}\chi_{\rm Mn}(j)$ which expresses the indirect effect of the external field on the holes spins. This term is negative, *i.e.* it favors the increased polarization of the charge carriers, whereas the small positive term, B_i, coming from the direct coupling to the external field, favors the hole depolarization.

The set of Eqs. (4.57) and (4.64) relate the susceptibilities $\chi_{\rm Mn}(i)$ and $\chi_h(i)$ to one another. The self consistent equation for determining $\chi_{\rm Mn}(i)$ at each site i can be derived by substituting (4.64) into (4.57):

$$\sum_j \left[\delta_{ij} + \beta\, R_{ij} B_s{}'(\beta H_i)\right]\ \chi_{\rm Mn}(j) = \beta\,(1+P_i) B_s{}'(\beta H_i) \tag{4.67}$$

where

$$R_{ij} = \sum_{n\sigma} f(E_{n\sigma}) \sum_{k\neq n} \frac{2Re\{J_{k\sigma,n\sigma}(i) J^*_{k\sigma,n\sigma}(j)\}}{E_{k\sigma} - E_{n\sigma}} + \beta \sum_{n\sigma} J_{n\sigma,n\sigma}(i) J_{n\sigma,n\sigma}(j) g(E_{n\sigma})$$

$$-\beta \frac{\sum_{n\sigma}\sum_{m\alpha}\sigma\alpha J_{n\sigma,n\sigma}(i) J_{m\alpha,m\alpha}(j) g(E_{n\sigma})\, g(E_{m\alpha})}{\sum_{n\sigma} g(E_{n\sigma})} \tag{4.68}$$

and

$$P_i = \frac{\beta}{2}\sum_{n\sigma} J_{n\sigma,n\sigma}(i) g(E_{n\sigma})\left\{1 - \sigma\frac{\sum_{m\alpha}\alpha g(E_{m\alpha})}{\sum_{m\alpha} g(E_{m\alpha})}\right\}. \tag{4.69}$$

Once we derive $\chi_{\rm Mn}(i)$, the values of $\chi_h(i)$ can be obtained from (4.64). Having the solutions at all sites $i = 1, ..., N_d$, we define $\chi_{\rm Mn} = \sum_i \chi_{\rm Mn}(i)/N_d$ and $\chi_h = \sum_i \chi_h(i)/N_d$ as the total Mn and hole susceptibilities in $4x(g\mu_B)^2/a^3$ units. Since there are fewer holes than Mn spins and also each Mn spin is five times bigger than a hole spin, we approximate the total susceptibility as being equal to the Mn spin contributions:

$$\chi_{total} = \chi_{\rm Mn} + \chi_h \approx \chi_{\rm Mn}.$$

When comparing susceptibilities with different concentration we divide χ_{total} by x and express it in x free unit $4(g\mu_B)^2/a^3$.

It is useful to compare the formalism developed here with the conventional statistical formula for static susceptibility, which within mean-field approximation is:

$$\chi' = \frac{\beta}{N_d}\sum_{ij}\{\langle S_i S_j\rangle - \langle S_i\rangle\langle S_j\rangle\} = \frac{1}{N_d}\sum_i \chi'_{\rm Mn}(i)$$

where

$$\chi'_{\rm Mn}(i) = \beta\{\langle S_i^2\rangle - \langle S_i\rangle^2\} = \beta B_s{}'(\beta H_i). \tag{4.70}$$

Comparing this line with Eq. (4.57) shows that this formula does not account for the effect that the supplementary polarization of the holes has on the Mn spin susceptibility. This is obvious since this statistical formula only considers direct coupling of the external field to the Mn spins and does not include the effective internal magnetic field $H_{int}(i) = -\sum_j J_{ij} s_h^H(j)$, as a source of external field dependence in free energy. Therefore it may only be used for models where the magnetic moments are interacting directly to one another.

There are, however, two regions where $\chi'_{\mathrm{Mn}}(i) \approx \chi_{\mathrm{Mn}}(i)$. One is at very low temperatures $T < T_p$ where the holes are already fully polarized and the supplementary external magnetic field has no effect on them. The second is for $T > T_c$, where all susceptibilities including $\chi_h(i)$ are fast approaching zero. However, to find the susceptibility near and below T_c one has to use the full formalism derived in this section.

Chapter 5

Results for the ordered case

In order to understand the effects of disorder, we must first know the behavior of the system in the absence of disorder, i.e. in an ordered case. The ordered case corresponds to having the Mn impurities placed in an ordered simple cubic lattice, with a superlattice constant $a_L = a/(4x)^{\frac{1}{3}}$. Strictly speaking, only concentrations x for which a_L is commensurate with the GaAs lattice constant a are physically acceptable. In the ordered case, translational symmetry implies $s_h(i) = s_h$, $S_{\rm Mn}(i) = S_{\rm Mn}$ for all sites i of the Mn superlattice. Then, the charge carrier part of the mean-field Hamiltonian (3.20) can be diagonalized in $\vec{k}$ space,

$$\mathcal{H}_{cc}^{HF} = \sum_{\vec{k}\sigma} E_{\vec{k}\sigma} c_{\vec{k}\sigma}^{\dagger} c_{\vec{k}\sigma} \tag{5.1}$$

where

$$E_{\vec{k}\sigma} = \epsilon_{\vec{k}} + \frac{J_0 S_{\rm Mn}}{2}\sigma \tag{5.2}$$

Here, $\epsilon_{\vec{k}} = \sum_{\vec{\delta}\neq 0} t_{\vec{\delta}} \exp(i\vec{k}\cdot\vec{\delta})$ is the kinetic energy of the non-interacting electrons, where $\vec{\delta}$ indexes all the neighboring sites and $t_{\vec{\delta}} = t_{ij}$ for which $|\vec{R}_i - \vec{R}_j| = |\vec{\delta}|$. Also, $J_0 = \sum_{\vec{\delta}} J_{\vec{\delta}}$, where $J_{\vec{\delta}} = J_{ij}$ for which $|\vec{R}_i - \vec{R}_j| = |\vec{\delta}|$. If N_d is the number of Mn spins, the spin expectation values at finite T are:

$$s_h = \frac{1}{2N_d}\sum_{\vec{k}\sigma} \sigma f(E_{\vec{k}\sigma}) \tag{5.3}$$

$$S_{\rm Mn} = B_S(-\beta J_0 s_h) \tag{5.4}$$

where $f(E_{\vec{k}\sigma})$ is the Fermi distribution, and the chemical potential μ is found from the condition $\sum_{\vec{k}\sigma} f(E_{\vec{k}\sigma}) = N_h$. At $T = 0$ the situation is even simpler. In this case, $f(E_{\vec{k}\sigma}) = \theta(k_F - |\vec{k}|)\delta_{\sigma\downarrow}$, where the Fermi momentum is given by $N_h = \sum_{|\vec{k}|<k_F} 1$. Since all spins are fully polarized, at $T = 0$ we find $s_h = -N_h/(2N_d) = -p/2$ whereas $S_{\rm Mn} = \frac{5}{2}$.

In the presence of a static external magnetic field, of interest for computation of the static susceptibility, these equations change to:

$$E_{\vec{k}\sigma}^{H} = \epsilon_{\vec{k}} + \frac{\sigma}{2}(J_0 S_{\rm Mn}^{H} - g\mu_b H) \tag{5.5}$$

$$s_h^{H} = \frac{1}{2N_d}\sum_{\vec{k}\sigma} \sigma f(E_{\vec{k}\sigma}^{H}) \tag{5.6}$$

$$S_{\rm Mn}^{H} = B_S\left(\beta(\tilde{g}\mu_b H - J_0 s_h^{H})\right). \tag{5.7}$$

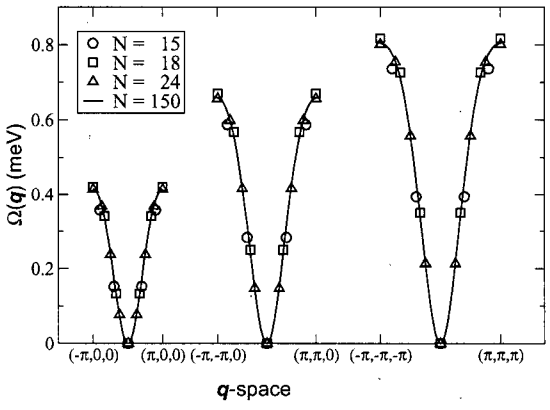

Figure 5.1: Spin-wave dispersion in the ordered case. Lattices of linear size $N = 15, 18, 24$ and 150, with respectively $N_d = 125, 216, 512$ and 125000 Mn spins are considered. This corresponds to $x = 0.0092$ and $p = 10\%$. Dispersion is plotted along $(-\pi, 0, 0) \rightarrow (\pi, 0, 0)$, $(-\pi, -\pi, 0) \rightarrow (\pi, \pi, 0)$ and $(-\pi, -\pi, -\pi) \rightarrow (\pi, \pi, \pi)$. From [15].

5.1 Dynamical transversal susceptibility

Since singularities in the transversal susceptibility are linked to the collective magnetic excitations (spin-waves), we first briefly consider their spectrum in the ordered case. Due to the invariance to superlattice translations, each spin-wave mode is indexed by a wavevector $\vec{Q}$ defining its spatial mode distribution, $Y_i \sim \delta S^+(i) \sim \exp(i\vec{Q} \cdot \vec{R}_i)$. We denote by $\hbar\omega_{\vec{Q}}$ the corresponding spin-wave energy. The spin-wave spectrum at $T = 0$ is then given by [15]:

$$\hbar\omega_{\vec{Q}} - \frac{pJ_0}{2} = -\frac{S|J(\vec{Q})|^2}{2N_d} \sum_{\vec{k}} \frac{f(E_{\vec{k},\downarrow})}{\hbar\omega_{\vec{Q}} + \epsilon_{\vec{k}-\vec{Q}} - \epsilon_{\vec{k}} + J_0 S} \tag{5.8}$$

where

$$J(\vec{Q}) = \sum_{\vec{\delta}} J_{\vec{\delta}} \exp(i\vec{Q} \cdot \vec{\delta}). \tag{5.9}$$

(This dispersion can be obtained from the RPA equations (4.20) and (4.21) in the absence of the external field, as we show in the following). For each value of $\vec{Q}$ this equation can be solved numerically. The resulting spin-wave dispersion along three different directions in the Brillouin zone is shown in Fig. 5.1. In the long wavelength limit $Q \rightarrow 0$, one can show that the expected magnon dispersion $\hbar\omega_{\vec{Q}} \sim Q^2$ is recovered [15].

We now discuss the dynamical transverse susceptibility in the ordered case. In the RPA response function equation (4.53), we found the magnetic response

$\delta S^+(i,\omega)$ to a general space dependent magnetic field $H^+(i,\omega)$. We begin by decomposing $H^+(i,\omega)$ into its Fourier components $H^+(\vec{q},\omega)$ as following:

$$H^+(i,\omega) = \frac{1}{\sqrt{N_d}} \sum_{\vec{q}} H^+(\vec{q},\omega)\ \exp(i\vec{q}\cdot\vec{R}_i). \tag{5.10}$$

Considering an external field with a particular wave vector $\vec{Q}$,

$$H^+(\vec{q},\omega) = \sqrt{N_d}\delta_{\vec{Q},\vec{q}} H^+(\omega),$$

the external field becomes:

$$H^+(i,\omega) = H^+(\omega)\exp(i\vec{Q}\cdot\vec{R}_i). \tag{5.11}$$

For this external magnetic field, the source term $B_i(\omega)$ [see Eq. (4.55)] becomes:

$$\begin{aligned} B_i(\omega) &= \exp(i\vec{Q}\cdot\vec{R}_i)\, H^+(\omega)\, S_{\mathrm{Mn}} \\ &\quad \times\Big\{1 + J(\vec{Q})\sum_{\vec{k}} \frac{f(E_{\vec{k}-\vec{Q},\uparrow}) - f(E_{\vec{k},\downarrow})}{\hbar\omega + \epsilon_{\vec{k}-\vec{Q}} - \epsilon_{\vec{k}} + J_0 S_{\mathrm{Mn}}}\Big\}. \end{aligned} \tag{5.12}$$

Since $B_i \sim \exp(i\vec{Q}\cdot\vec{R}_i)$, the solutions of the RPA response equation (4.53), $\delta S^+(i,\omega)$, should also have the same form,

$$\delta S^+(i,\omega) = \delta S^+(\vec{Q},\omega)\exp(i\vec{Q}\cdot\vec{R}_i). \tag{5.13}$$

and the RPA equation (4.53) reduces to:

$$\begin{aligned} &\Big\{(\hbar\omega - J_0 s_h) - \frac{S_{\mathrm{Mn}}|J(\vec{Q})|^2}{2N_d}\sum_{\vec{k}} \frac{f(E_{\vec{k}-\vec{Q},\uparrow}) - f(E_{\vec{k},\downarrow})}{\hbar\omega + \epsilon_{\vec{k}-\vec{Q}} - \epsilon_{\vec{k}} + J_0 S_{\mathrm{Mn}}}\Big\}\delta S^+(\vec{Q},\omega) \\ &\qquad = H^+(\omega) S_{\mathrm{Mn}}\Big\{1 + J(\vec{Q})\sum_{\vec{k}} \frac{f(E_{\vec{k}-\vec{Q},\uparrow}) - f(E_{\vec{k},\downarrow})}{\hbar\omega + \epsilon_{\vec{k}-\vec{Q}} - \epsilon_{\vec{k}} + J_0 S_{\mathrm{Mn}}}\Big\} \end{aligned} \tag{5.14}$$

This allows us to solve directly for $\delta S^+(\vec{Q},\omega)$ and thus to find the dynamic magnetic susceptibility (in units of $4x(g\mu_b)^2/a^3$)

$$\delta S^+(\vec{Q},\omega) = \chi(\vec{Q},\omega) H^+(\omega) \tag{5.15}$$

to be given by:

$$\chi(\vec{Q},\omega) = \frac{S_{\mathrm{Mn}}\Big\{1 + J(\vec{Q})\sum_{\vec{k}} \frac{f(E_{\vec{k}-\vec{Q},\uparrow}) - f(E_{\vec{k},\downarrow})}{\hbar\omega + \epsilon_{\vec{k}-\vec{Q}} - \epsilon_{\vec{k}} + J_0 S_{\mathrm{Mn}}}\Big\}}{(\hbar\omega - J_0 s_h) - \frac{S_{\mathrm{Mn}}|J(\vec{Q})|^2}{2N_d}\sum_{\vec{k}} \frac{f(E_{\vec{k}-\vec{Q},\uparrow}) - f(E_{\vec{k},\downarrow})}{\hbar\omega + \epsilon_{\vec{k}-\vec{Q}} - \epsilon_{\vec{k}} + J_0 S_{\mathrm{Mn}}}} \tag{5.16}$$

By comparing this expression against Eq. (5.8), we see that indeed the susceptibility becomes singular when $\omega = \omega_{\vec{Q}}$ of a spin-wave (as already discussed,

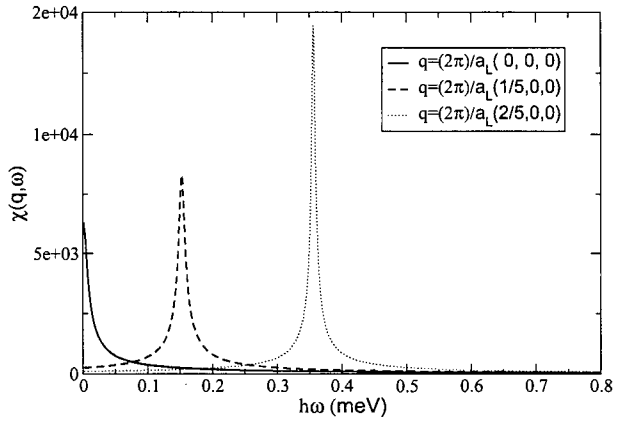

Figure 5.2: The dynamic susceptibility $\chi(\vec{q},\omega)$ at $T = 0$ for an ordered system with $N_d = 125$ spins, for $x = 0.00926$ and $p = 10\%$. The three lines correspond to the allowed values $\vec{q} = (0,0,0)$ (full line), $\frac{2\pi}{a_L}(\frac{1}{5},0,0)$ (dashed line) respectively $\frac{2\pi}{a_L}(\frac{2}{5},0,0)$ (dotted line).

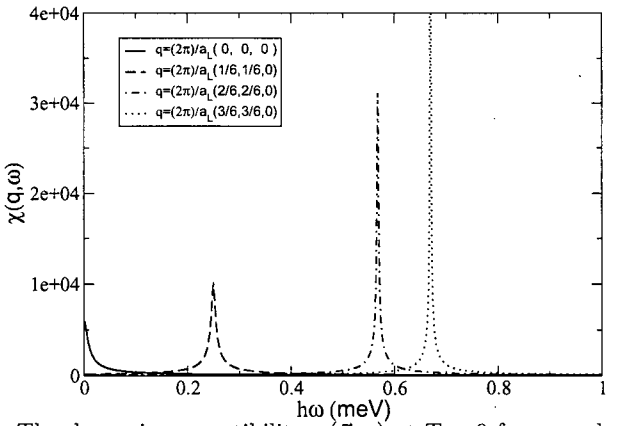

Figure 5.3: The dynamic susceptibility $\chi(\vec{q},\omega)$ at $T = 0$ for an ordered system with $N_d = 216$ spins, for $x = 0.00926$ and $p = 10\%$. The four lines correspond to the allowed values $\vec{q} = (0,0,0)$ (full line), $\frac{2\pi}{a_L}(\frac{1}{6},\frac{1}{6},0)$ (dashed line), $\frac{2\pi}{a_L}(\frac{2}{6},\frac{2}{6},0)$ (dot-dash line) respectively $\frac{2\pi}{a_L}(\frac{3}{6},\frac{3}{6},0)$ (dotted line).

at $T = 0$, $s_h = -p/2$, $S_{\mathrm{Mn}} = S$). Equation (5.16) can be further simplified for

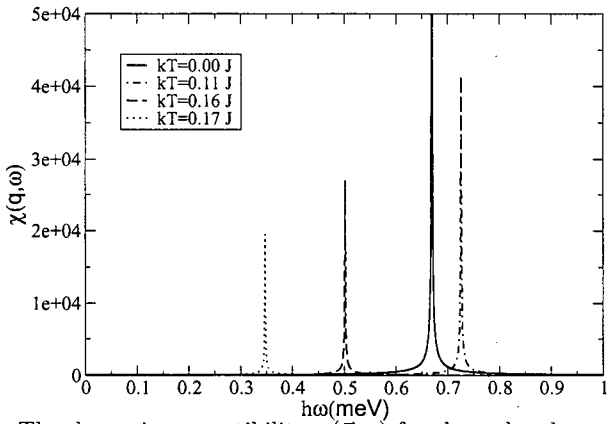

Figure 5.4: The dynamic susceptibility $\chi(\vec{q},\omega)$ for the ordered case, with $N = 18$, $N_d = 216$ Mn spins and $p = 0.10$. We choose $\vec{q} = \frac{2\pi}{a_L}(\frac{1}{2},\frac{1}{2},0)$, and plot the susceptibility at four different temperatures, $KT/J = 0, 0.11, 0.16$ and 0.17.

a homogeneous magnetic field, $\vec{Q} = 0$, where we find:

$$\chi(0,\omega) = \frac{S_{\rm Mn}}{\hbar\omega}. \tag{5.17}$$

This becomes singular for $\hbar\omega = 0$. This is due to the fact that the corresponding spin-wave energy for the $\vec{Q} = 0$ mode is zero. This mode is the Goldstone boson, since due to rotational symmetry there is no energy cost for a global rotation of all the Mn spins.

In Figs. 5.2 and 5.3 we plot $\chi(\vec{q},\omega)$ at $T = 0$ for systems with linear sizes $N = 15$, respectively $N = 18$, for certain allowed wavevectors in the Brillouin zone. The peaks in each $\chi(\vec{q},\omega)$ susceptibility clearly match to the energy of the spin-wave mode with the same $\vec{q}$, plotted in Fig. 5.1.

In Fig. 5.4 we show $\chi(\vec{q},\omega)$ vs. ω at a fixed momentum $\vec{q} = \frac{2\pi}{a_L}(\frac{1}{2},\frac{1}{2},0)$ for four different temperature, $k_BT = 0J$, $0.11J$, $0.16J$, $0.17J$. We observe that the energy of the spin-wave mode $\hbar\omega_{\vec{q}}$, signalled by the singularity, first increases with increasing T, but at temperatures closer to the critical temperature it starts to decrease towards $\omega = 0$. This behavior is demonstrated more clearly in Fig. 5.5, where we plot the variation of the spin-wave energy $\hbar\omega_{\vec{q}}$ with the temperature, for three different values of $\vec{q}$ corresponding to a lattice size $N = 18$. The initial increase with increasing temperature is due to the decrease of the Mn spin expectation value from $S_{\rm Mn} = 5/2$ at $T = 0$ to a lower value at higher temperatures [see Eq. (5.8), (5.16)]. However, closer to the critical temperature both s_h and the energy gap between spin-up and spin-down states decrease, leading to a decrease of the spin-wave energies.

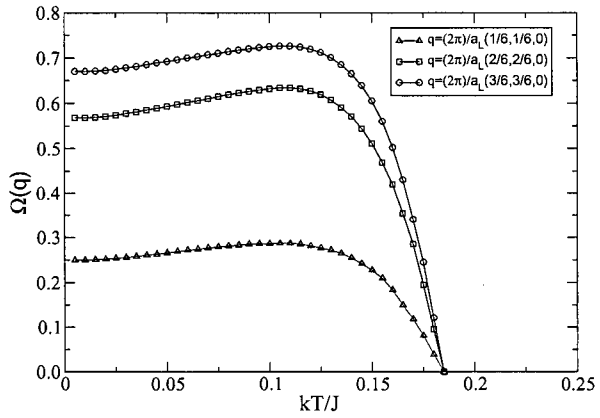

Figure 5.5: Temperature dependence of the spin-wave energies (position of singularity in $\chi(\vec{q},\omega)$) for three different wavevectors $\vec{q} = \frac{2\pi}{a_L}(\frac{1}{6},\frac{1}{6},0)$, $\frac{2\pi}{a_L}(\frac{2}{6},\frac{2}{6},0)$ respectively $\frac{2\pi}{a_L}(\frac{3}{6},\frac{3}{6},0)$. Parameters are $N = 18$, $N_d = 216$ Mn spins and $p = 10\%$.

5.2 Static longitudinal susceptibility

In this section we derive a simple formula for the static longitudinal susceptibility in an ordered system. We cannot directly use the results derived in Section (4.3) for this susceptibility, because there we used non-degenerate perturbation theory for the derivation. In the ordered case, electronic levels $E_{\vec{k}\sigma}$ for $k \neq 0$ are degenerate due to various symmetries of the Brillouin zone. This degeneracy has to be taken into account, but otherwise the procedure closely mirrors that used in Section (4.3).

We start with the self-consistent equations in the presence of a static magnetic field, Eqs. (5.5), (5.6) and (5.7). The goal is to expressed the Mn and hole susceptibilities:

$$\chi_{\mathrm{Mn}} = \left.\frac{dS^H_{\mathrm{Mn}}}{dH}\right|_{H=0} \qquad \chi_h = \left.\frac{ds^H_h}{dH}\right|_{H=0},$$

in terms of the mean-field solutions in the absence of magnetic field, given by equations (5.2), (5.3) and (5.4).

As the first step we take the derivative with respect to H from (5.7) to find:

$$\chi_{\mathrm{Mn}} = \beta\,(1 - J_0\,\chi_h)\,B_S{}'(-\beta J_0 s_h) \tag{5.18}$$

where $B'_S(x) = d/dx B_S(x)$ and again we set $g\mu_B = 1$ for convenience. In order to find the second equation linking χ_h to χ_{Mn}, we start by finding the first order variation with H of the charge carrier eigenenergies, which follows directly from

(5.5) to be:

$$E_{n\sigma}^{(1)} = \left.\frac{dE_{n\sigma}^{H}}{dH}\right|_{H=0} = \frac{\sigma}{2} J_0 \chi_{\rm Mn} - \frac{\sigma}{2}. \tag{5.19}$$

The variation with H of the chemical potential is given by [see Eq. (4.62)]

$$\left.\frac{d\mu(H)}{dH}\right|_{H=0} = \frac{\sum_{n\sigma} E_{n\sigma}^{(1)}\, g(E_{n\sigma})}{\sum_{n\sigma} g(E_{n\sigma})} \tag{5.20}$$

where $g(x)$ is the derivative of the Fermi distribution $f(x)$. Finally, the hole susceptibility χ_h can be related to $\chi_{\rm Mn}$ by taking the derivative of Eq. (5.6):

$$\chi_h = \frac{\beta}{2N_d} \sum_{n\sigma} \sigma \left(E_{n\sigma}^{(1)} - \frac{d\mu}{dH} \right) g(E_{n\sigma}). \tag{5.21}$$

Using Eqs. (5.19) and (5.20), this can be written in the simpler form:

$$\chi_h = \beta\gamma(J_0 \chi_{\rm Mn} - 1), \tag{5.22}$$

where

$$\gamma = \frac{1}{4\,N_d} \left\{ \frac{[\sum_{n\sigma} g(E_{n\sigma})]^2 - [\sum_{n\sigma} \sigma g(E_{n\sigma})]^2}{\sum_{n\sigma} g(E_{n\sigma})} \right\}. \tag{5.23}$$

Substituting Eq. (5.22) into Eq. (5.18), we find the Mn susceptibility to be given by:

$$\chi_{\rm Mn} = \frac{\beta(1+\beta J_0 \gamma)\, B_s{}'(-\beta J_0 s_h)}{1 + (\beta J_0)^2\, \gamma\, B_s{}'(-\beta J_0 s_h)}. \tag{5.24}$$

which allows us to find the hole susceptibility χ_h as:

$$\chi_h = -\beta\gamma \left[\frac{1 - J_0 \beta B_s{}'(-\beta J_0 s_h)}{1 + (\beta J_0)^2\, \gamma\, B_s{}'(-\beta J_0 s_h)} \right]. \tag{5.25}$$

These static longitudinal susceptibilities are plotted as a function of temperature in Fig. 5.6. As expected, the critical temperature T_C is marked by singularities in these quantities.

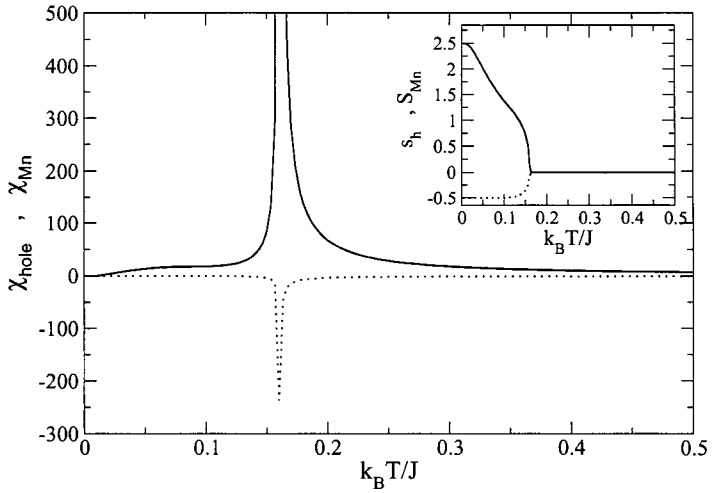

Figure 5.6: Mn and charge carrier static longitudinal susceptibilities as a function of T, for an ordered Mn configuration with $x = 0.00926$ and $p = 10\%$. The sample has a linear size $N = 24$ corresponding to $N_d = 512$. The inset shows the Mn and charge carrier magnetizations for the same configuration.

Chapter 6

The effect of disorder: numerical results

Disorder was previously shown to increase the critical temperature [11] and to broaden the spin-wave spectrum [15]. This suggests that disorder should also have a significant influence on the magnetic response functions. In this chapter we analyze and interpret the effects of disorder on the magnetic susceptibilities.

6.1 Dynamical susceptibility

We study three types of disorder – weak, moderate and full disorder, as defined in Section 3. We adopt the notation $\chi_o(\vec{q},\omega)$, $\chi_w(\vec{q},\omega)$, $\chi_m(\vec{q},\omega)$ and $\chi_f(\vec{q},\omega)$ to refer to ordered, respectively the weak, moderate and full disorder dynamical susceptibilities. Consistent with the last section and Ref. [15], we consider samples with a Mn concentration $x = 0.0092$ and different sizes $N_d = 125, 216$ and 512. Peaks in $\chi(\vec{q},\omega)$ are directly linked to the spin-wave eigenenergies for the corresponding degree of disorder. We therefore begin this section with a short review of the effects of disorder on the spin-wave spectrum [15].

In Fig. 6.1 we show the spin-wave spectrum density of states (DOS) at $T = 0$ for ordered, moderate and full disorder configurations. Disorder significantly broadens the density of states and considerable weight is transferred both to lower and to higher energies (notice that the scale in Fig. 6.1 is logarithmic). One important effect discussed in Ref. [15] is that disorder leads to localization of the spin-wave modes in the high and low-energy regimes.

For full disorder configurations and the parameters considered, localization of the spin-wave modes occurs in the $E > 1$ meV and $E < 5 \times 10^{-3}$ meV ranges. The localized modes in the low energy regime $E < 5 \times 10^{-3}$ meV, which is more visible for the highest degree of disorder, are individual spin-flips of quasi-free Mn spins which are far from the regions where the holes are located. The localized modes in the high energy region $E > 1$ meV, which occur for both moderate and full disorder, are related to spin-flips inside strongly coupled clusters of Mn spins, where the holes are located with a high probability. The dynamical susceptibility is expected to show singularities at frequencies equal to those of spin-waves that can be excited by the external magnetic field. As a result, both the broadening of the spin-wave spectrum, and the appearance of localized spin-wave modes with increasing disorder, should be signalled by changes in the dynamical susceptibility.

The method to compute the dynamical susceptibility was described in detail in Sec. (4.2). We briefly review it here. For each given disorder realization,

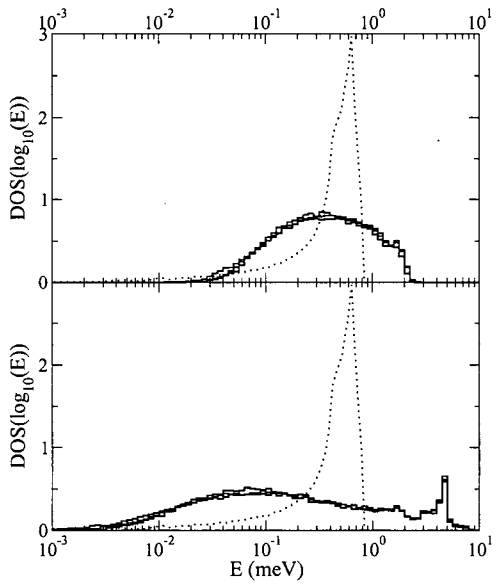

Figure 6.1: Average density of states $\rho(\log_{10} E)$ *on a logarithmic scale* for systems with $N_d = 125, 216$ and 512 Mn spins in moderately/full disordered configurations (upper/lower panels, full lines). The dotted line is the spin-wave density of states of a DMS with fully ordered (superlattice) configuration of Mn spins. All samples correspond to $x = 0.00924$, $p = 10\%$. From Ref. [15].

the first step is to find the self-consistent Hartree-Fock solution. We compute the matrix $\mathbf{M}(\omega)$ [Eq. (4.54)] and the vector $\mathbf{B}(\omega)$ [Eq. (4.55)] corresponding to an external magnetic field $h_i^+(\omega) = \exp(i\vec{q}\cdot\vec{R}_i)$ where $\vec{q}$ is a wave vector in the Brillouin zone consistent with the boundary conditions of the ordered Mn superlattice with $a_L = a/(4x)^{\frac{1}{3}} = 3a$ ($x = 0.0092$). We then solve the inhomogeneous system of linear equations (4.53) to find $\delta S_i^+(\omega)$ for each site $i = 1, .., N_d$. The dynamical susceptibility is then calculated from Eq. (4.24), by averaging over results from many disorder realizations. It is proportional to the average amplitude of the spins' precessional motion in the transversal direction. $\chi(\vec{q},\omega)$ can also be related to the energy absorbed by the DMS from the external magnetic field through the fluctuation-dissipation theorem.

The dynamical susceptibility $\chi_o(\vec{q},\omega)$ for the ordered superlattice case was analyzed in Section (5.1) of the previous chapter [see Figs. 4.19, 4.20, 4.21]. It has singularities for frequencies in the spin-wave spectrum $\omega = \omega_{\vec{q}}$, as expected

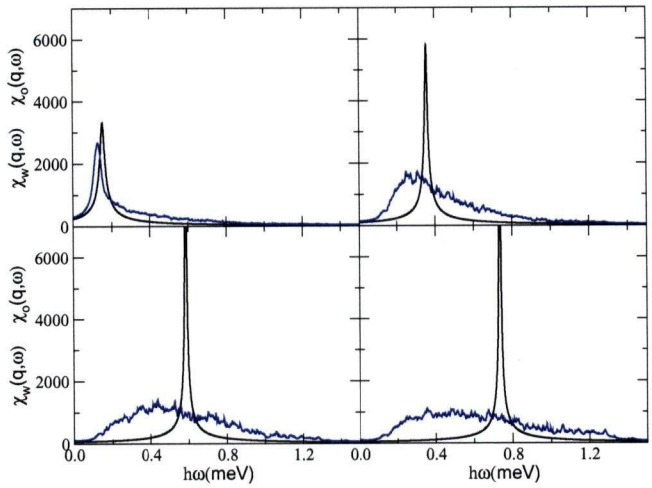

Figure 6.2: The dynamical susceptibility for ordered (black) and weakly disordered (blue) Mn configurations at $T = 0$, for $x = 0.00924$, $p = 0.10$, $N = 15$. Panels correspond to $\vec{q}_1 = \frac{2\pi}{a_L}(\frac{1}{5}, 0, 0)$ (upper left); $\vec{q}_2 = \frac{2\pi}{a_L}(\frac{2}{5}, 0, 0)$ (upper right); $\vec{q}_3 = \frac{2\pi}{a_L}(\frac{2}{5}, \frac{2}{5}, 0)$ (lower left) and $\vec{q}_4 = \frac{2\pi}{a_L}(\frac{2}{5}, \frac{2}{5}, \frac{2}{5})$ (lower right).

from the conservation of energy and momentum. It should be noticed, however, that as we go to full disorder, the Mn superlattice with $a_L = 3a$ and its related Brillouin $\vec{q}$-space loose their relevance, since translational invariance is broken and the quasimomentum $\vec{q}$ is no longer a good quantum number for any individual disorder realization. Average over all disorder realizations restores the translational invariance, but now corresponding to translations on the original FCC Ga lattice. As a result, $\vec{q}$-vectors of the original FCC lattice with lattice spacing a should be used. However, we will only consider vectors in the $\vec{q}$-space of the ordered Mn superlattice with $a_L = 3a$ even for the full disorder case, $\chi_f(\vec{q}, \omega)$. The reasons are three-fold. First, the $\vec{q}$-space of the Mn superlattice with $a_L = 3a$ is a subspace of the $\vec{q}$-space of the original lattice with lattice distance a. Secondly, this allows us to compare the effects of disorder at a given value of $\vec{q}$, from fully ordered to fully disordered configurations. Finally, as we show below, in the fully disordered case, $\chi_f(\vec{q}, \omega)$ becomes roughly independent of $\vec{q}$. As a result, investigating the behavior of $\chi_f(\vec{q}, \omega)$ at other values of $\vec{q}$ would not reveal additional information. A second computational issue that has to be addressed is the value of the small parameter η, which cannot be set to zero in the numerical computations. A finite η is physically linked to a finite lifetime of the spin-wave modes, due to scattering on other spin-waves (such processes are neglected at the RPA level). The value of η only affects the height and width

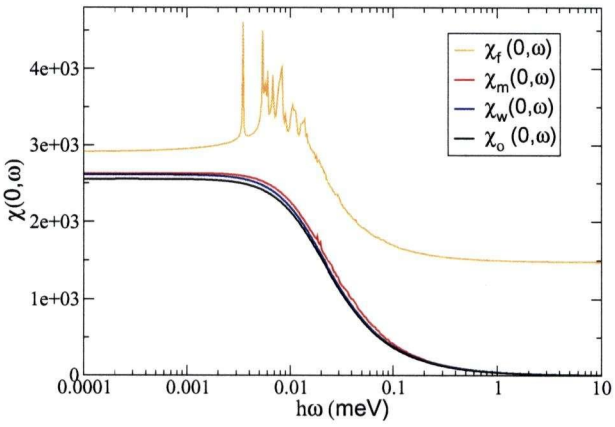

Figure 6.3: Comparison of dynamical susceptibilities in the homogeneous case. Only for full disorder we see some variations from the expected $\chi_o(0,\omega) = \frac{S_{\rm Mn}}{\hbar\omega}$ behavior [Eq. (5.17)]. The $\omega \to 0$ divergence is cut-off by the finite value for η used in the numerical computations.

of peaks associated with excitation of spin-wave modes in the system by the external magnetic field. In this study, we use the value $\eta = 0.02J$ for $\chi_o(\vec{q},\omega)$ and $\eta = 0.05J$ for $\chi_w(\vec{q},\omega)$, $\chi_m(\vec{q},\omega)$ and $\chi_f(\vec{q},\omega)$.

We start our analysis on the effects of disorder by comparing $\chi_w(\vec{q},\omega)$ and $\chi_o(\vec{q},\omega)$ at $T = 0$ for samples with linear size $N = 15$ ($N_d = 125$ Mn spins). This is shown in Fig. 6.2 for four different wave vectors: $\vec{q}_1 = \frac{2\pi}{a_L}(\frac{1}{5},0,0)$, $\vec{q}_2 = \frac{2\pi}{a_L}(\frac{2}{5},0,0)$, $\vec{q}_3 = \frac{2\pi}{a_L}(\frac{2}{5},\frac{2}{5},0)$ and $\vec{q}_4 = \frac{2\pi}{a_L}(\frac{2}{5},\frac{2}{5},\frac{2}{5})$ consistent with the system size considered. The weak-disorder results correspond to an average over 15 different disorder realizations. The vectors $\vec{q}_i$, $i = 1,..,4$ are chosen in order of increasing magnitude, such that the corresponding spin-wave modes $\omega_{\vec{q}}$ of the ordered superlattice are also in increasing order.

In the ordered case, the dynamic susceptibility has a single singularity at $\omega = \omega_{\vec{q}}$. In a disordered case, for each individual disorder realization we see multiple peaks in $\chi_w(\vec{q},\omega)$, since the momentum $\vec{q}$ is no longer a good quantum number of the spin-wave modes, and therefore the external magnetic field can excite many such modes. Averaging over many disorder configurations partially smoothes-out such individual peaks corresponding to different spin-waves, although their signatures can still be seen in Fig. 6.2. Overall, the susceptibility now exhibits a broader peak. In each case we observe that this broad peak in $\chi_w(\vec{q},\omega)$ is displaced from the corresponding ordered $\omega_{\vec{q}}$ value towards lower energies. This is consistent with the previous observation that increased disorder leads to increased weight for low-energy spin-waves. Another important aspect is that as we go to larger values of $\vec{q}$, the broad peak of $\chi_w(\vec{q},\omega)$ becomes even broader. The physical reason for this broadening is that the presence of the weak disorder is more acutely felt at shorter wavelengths. The effect of disorder

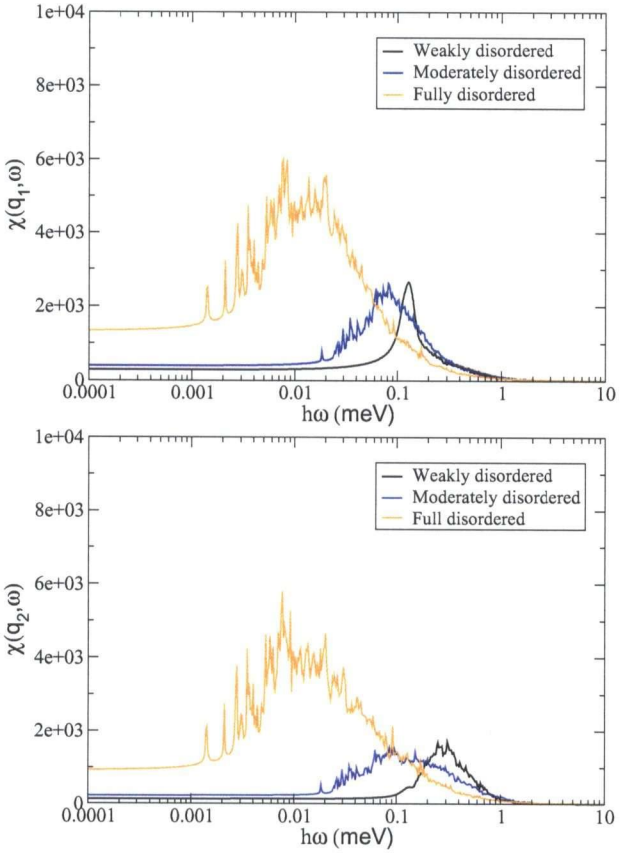

Figure 6.4: The dynamic susceptibility for three types of disorder, at $T = 0$. The upper graph corresponds to $\vec{q} = \frac{2\pi}{a_L}(\frac{1}{5}, 0, 0)$, the lower one corresponds to $\vec{q} = \frac{2\pi}{a_L}(\frac{2}{5}, 0, 0)$. All samples have $N = 15$, $N_d = 125$, $x = 0.00926$ and $p = 10\%$.

is least important for spatially homogeneous fields with $\vec{q} = 0$. In this case,

$$\chi_m(0,\omega) \approx \chi_w(0,\omega) \approx \chi_o(0,\omega) = \frac{S_{\mathrm{Mn}}}{\hbar\omega}$$

and only for full disorder we see some variations in $\chi_f(0,\omega)$, shown in Fig. 6.3.

As the next step we investigate higher degrees of disorder. In Figs. 6.4 we show the susceptibilities $\chi_w(\vec{q},\omega)$, $\chi_m(\vec{q},\omega)$ and $\chi_f(\vec{q},\omega)$ for two different wave vectors, $\vec{q}_1 = \frac{2\pi}{a_L}(\frac{1}{5}, 0, 0)$ and $\vec{q}_2 = \frac{2\pi}{a_L}(\frac{2}{5}, 0, 0)$, on a logarithmic energy scale. In order to reach to bulk limit, for each susceptibility plotted in Fig. 6.4, we averaged over 20 different disorder realizations. We see that as we go to higher disorder, the peak in the dynamical magnetic susceptibility shifts to

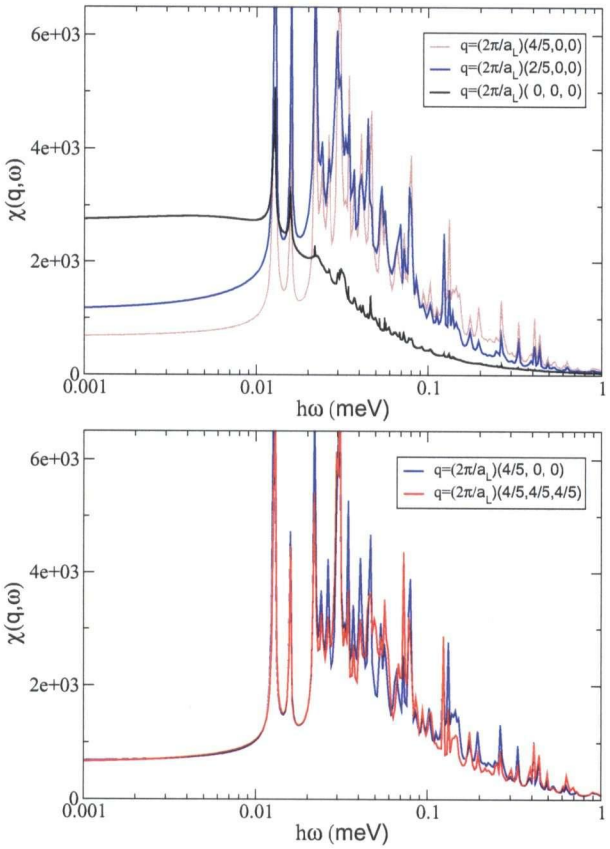

Figure 6.5: $\chi_f(\vec{q},\omega)$ for four values of $\vec{q}$, corresponding to the same *individual* Mn disorder realization. The upper panel shows three smaller $\vec{q}$ values while the lower panel compares $\chi_f(\vec{q},\omega)$ for two larger $\vec{q}$ values.

lower energies and becomes broader. These changes are more pronounced for higher levels of disorder. Also notice that $\chi_f(\vec{q}_1,\omega) \approx \chi_f(\vec{q}_2,\omega)$. As we show in the following, $\chi_f(q,\omega)$ is roughly independent on the value of $\vec{q}$, when $\vec{q}$ is large.

In Fig. 6.5 we show $\chi_f(\vec{q},\omega)$ for four values of $\vec{k}$. All curves are for the same individual Mn disorder realization (not the bulk limit). The upper panel shows $\chi_f(\vec{q},\omega)$ for three smaller values of $\vec{q}$ and the lower panel shows $\chi_f(\vec{q},\omega)$ for two larger values of $\vec{q}$. We observe that the individual spin-wave peaks in $\chi_f(\vec{q},\omega)$ for various finite $\vec{q}$ occur exactly at same values of energy, since they all couple to the same spin-wave modes. The differences between curves corresponding to different $\vec{q}$ are mostly in the amplitude of peaks corresponding to various spin-wave excitations (peaks become sharper for lower wavelengths). There are

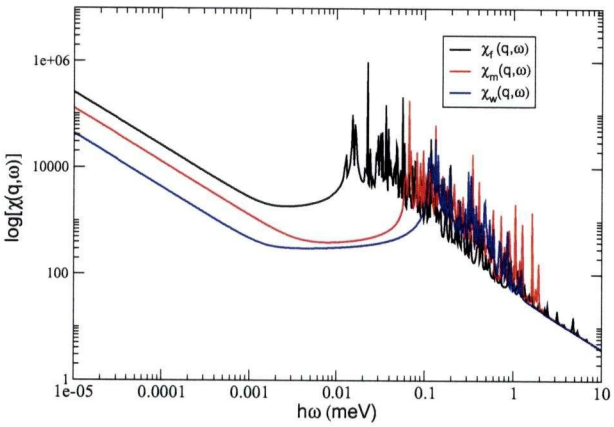

Figure 6.6: $\log[\chi(\vec{q},\omega)]$ for three levels of disorder, for $\vec{q} = \frac{2\pi}{a_L}(\frac{1}{5},0,0)$, $\eta = 0$, $p = 0.1$ and $x = 0.092$. Curves are for individual disorder realizations.

noticeable changes in $\chi_f(\vec{q},\omega)$ in the limit $|\vec{q}| \to 0$. In this limit, individual peaks still appear at the same frequencies as before, but they become weaker and some fade away (upper panel). Even such differences become less noticeable for higher $\vec{q}$ values (lower panel). Therefore we conclude that $\chi_f(\vec{q},\omega)$ is roughly independent of $\vec{q}$, for finite $\vec{q}$.

As already discussed, as disorder increases we see the signature of all the spin-waves in the dynamical susceptibility. This is also true for the Goldstone mode, $\hbar\omega = 0$. In the ordered case, coupling to this mode occurs only for a homogeneous field $\vec{q} = 0$, in which case $\chi_o(0,\omega) = S_{\rm Mn}/\hbar\omega$. For any other value of $\vec{q}$, $\chi_o(\vec{q},0) = 0$ (see previous section). In the disordered cases, however, coupling to the Goldstone mode is seen for all finite values of $\vec{q}$ as well. This is not apparent for the results shown so far, since they correspond to a finite value of η which removes the singularity. However, in Fig. 6.6 we plot $\log[\chi(\vec{q},\omega)]$ versus $\hbar\omega$ on logarithmic energy scale for three individual disorder realizations, for $\eta = 0$. From the linear behavior $\log[\chi(\vec{q},\omega)] \sim -\log[\hbar\omega]$ in the $\hbar\omega \to 0$ limit, we conclude that the dynamic susceptibility in the disordered cases has an asymptotic limit of the type $\alpha/(\hbar\omega)$. Fig. 6.6 also confirms that increasing levels of disorder lead to a wider spectrum of finite-energy spin-waves, at both lower and higher energies.

Fig. 6.6 also shows that for a finite $\vec{q}$, the value of α decreases with decreasing disorder, as expected since in the ordered case we must have $\alpha = 0$ (no coupling to the Goldstone boson for finite $\vec{q}$, and therefore no $\omega \to 0$ singularity). The value of α can also be inferred for the curves corresponding to finite η values, since in that case the singularity $\alpha/(\hbar\omega + i\eta)$ saturates to a value α/η as $\omega \to 0$. For example, in Fig. 6.3 corresponding to $\vec{q} = 0$, one can see that $\alpha \to S_{\rm Mn}$ as the amount of disorder is decreased. On the other hand, Fig. 6.5 shows that for a given disorder realization, the value of α decreases as $\vec{q}$ is increased

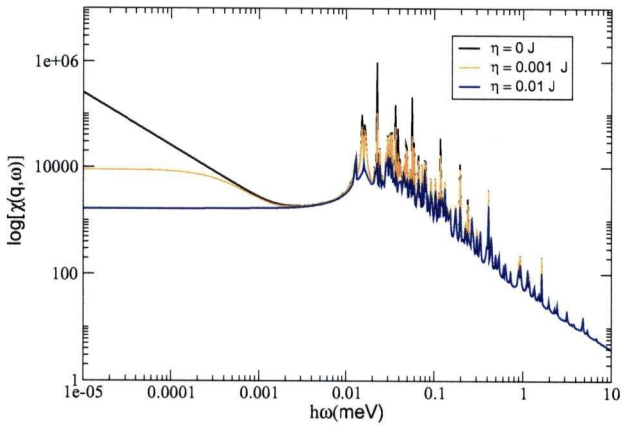

Figure 6.7: $\log[\chi_f(\vec{q},\omega)]$ for values of $\vec{q}$, p and x as in Fig. 6.6 and different η values. Curves are for individual disorder realizations.

(upper panel), converging to a finite value α_f for large $\vec{q}$ (lower panel). Later on we discuss finite-size effects, and demonstrate that the value α_f increases with the system size (for example Fig. 6.9). This strongly suggests that the coupling to the Goldstone mode is a bulk effect. It can only be prevented from observation by a finite spin-wave lifetime corresponding to a finite value of η, as demonstrated in Fig. 6.7. The effect of a finite η value is to remove the Goldstone mode singularity and to decrease and broaden the peaks corresponding to coupling to the finite-energy spin-waves.

In Fig. 6.8, $\chi_f(\vec{q},\omega)$ is shown for two different sizes, $N = 15$ ($N_d = 125$) in the upper panel and $N = 18$ ($N_d = 216$) in the lower panel. For each size the number of spin-wave excitations is equal to N_d. In order to have averages over similar numbers of spin-waves, we average over 20 and 40 different Mn spins configurations for $N = 18$ and $N = 15$ respectively. In both cases we see excitations near $\hbar\omega \sim 5$ meV. These excitations are related to high energy localized modes in the spin-wave DOS associated with nearest-neighbor Mn clusters [15], signalled by a peak in the DOS of Fig. 6.1. It is apparent that only a few peaks occur close to the lower and upper energy cut-offs, where the spin-wave density of states goes to zero. On the other hand, many peaks with large amplitude appear in the energy range where the DOS is maximum. All these facts show that the dynamical susceptibility calculated here is fully consistent with the spin-wave spectrum observations, discussed in Ref. [15].

In Ref. [15], the importance of size effects regarding the spin-wave states has been studied by examining three different sizes, $N = 15, 18$ and 24. The overall size-effects on the spin-wave DOS was found to be negligible as the DOS curves for these three sizes are very similar to one another (see Fig. 6.1). One size effect is that increase in the size N shifts the lower cutoff of the spin-wave spectrum to lower values of energy. These observations are consistent with our results for

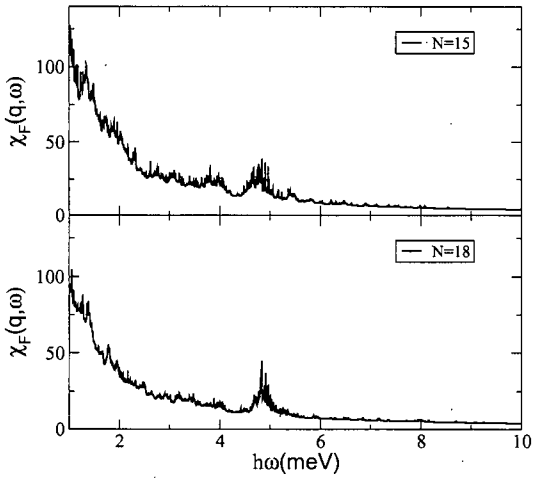

Figure 6.8: $\chi_f(\vec{q},\omega)$ for two system sizes, at $T = 0$. The upper panel is for $N = 15$, $N_d = 125$ Mn spins and $\vec{q} = \frac{2\pi}{a_L}(\frac{2}{5}, \frac{2}{5}, \frac{2}{5})$. The lower panel is for $N = 18$, $N_d = 216$ Mn spins and $\vec{q} = \frac{2\pi}{a_L}(\frac{2}{6}, \frac{2}{6}, 0)$. All samples have $x = 0.00926$ and $p = 10\%$.

the dynamical susceptibility. Since different sizes have different allowed $\vec{q}$-values, consistent with their boundary conditions, it is not possible to compare $\chi(\vec{q},\omega)$ for two different size for the same value of $\vec{q}$. However, as we mentioned before, in the fully-disordered case, the susceptibility is roughly independent on $\vec{q}$ for large enough values, and therefore we can make meaningful comparisons. The curves in Fig. 6.8 show very similar values for the dynamical susceptibilities corresponding to two different system sizes, implying small finite-size effects. On a logarithmic scale, we can also clearly see the the lower cutoff in energy shifts to lower values for larger system sizes (see Fig. 6.9). Thus, we find full agreement with the expectations based on the spin-wave DOS investigation.

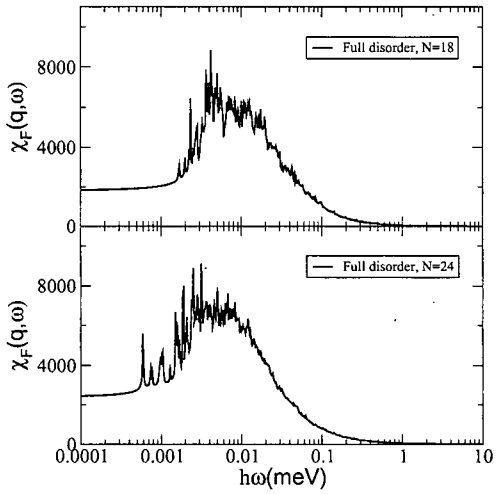

Figure 6.9: $\chi_f(\vec{q},\omega)$ for two system sizes, at $T = 0$. The upper panel is for $N = 18$, $N_d = 216$ Mn spins and $\vec{q} = \frac{2\pi}{a_L}(\frac{1}{6}, 0, 0)$. The lower panel is for $N = 24$, $N_d = 512$ Mn spins and $\vec{q} = \frac{2\pi}{a_L}(\frac{1}{8}, 0, 0)$. All samples have $x = 0.00926$ and $p = 10\%$.

6.2 Static Magnetic Susceptibility

In this section we study the effects of disorder on the static magnetic susceptibility and its temperature dependence. The majority of the data is for a concentration $x = 0.092$. The disorder is characterized by the minimum distance d_{min} allowed between any two Mn spins, $0.5 \leq d_{min} \leq 3$. The cases $d_{min} = 3$, respectively $d_{min} = 0.5$, correspond to the fully ordered, respectively fully disordered configurations.

The method to compute the longitudinal susceptibility $\chi_{\rm Mn}(i)$ of the Mn spin at each site $i = 1, .., N_d$ was described in Section 4.3. Here, when comparing susceptibilities for the same concentration x, we define $\chi = \sum_i \chi_{\rm Mn}(i)/N_d$, i.e. express susceptibilities in units of $4x(g\mu_B)^2/a^3$. When comparing results for different concentrations x, we will show χ_{total}/x, which is therefore measured in x-independent units of $4(g\mu_B)^2/a^3$.

The computation based on solving Eq. (4.67) can only be efficiently used for smaller samples (up to $N_d \approx 125$), since the calculation of the matrix elements R_{ij} in equation (4.67) becomes very time-consuming as the number of spins increases. For larger samples we use another method to calculate the longitudinal susceptibility, based directly on the definition

$$\chi \approx \left.\frac{S^H_{\rm Mn} - S_{\rm Mn}}{H}\right|_{g\mu_B H \ll 1} \tag{6.1}$$

where $S^H_{\rm Mn}$ and $S_{\rm Mn}$ are the average spin with and without the static magnetic field. These quantities can be directly computed self-consistently through iterations, as described in Section 3. Again, we measure χ in units of $4x(g\mu_B)^2/a^3$.

The only issue for using definition (6.1) directly is related to the proper value for H to be used, and the proper choice for the self-consistency criterion for a small but finite H. The definition (6.1) become precise for $H \to 0$, which suggests that we should use very small values for H. In turn, however, this requires the computation of $S_{\rm Mn}$ and $S^H_{\rm Mn}$ to very high accuracy, so that the errors in the nominator of Eq. 6.1 are small relative to the small value of H in the denominator. We have found that we obtain good agreement between the two methods if we choose $H = 10^{-4}$ meV and we define the self-consistency condition to be that the variation of the total magnetization in successive iterations is less than 10^{-6}. Even though achieving such a stringent criterion for self-consistency is quite time consuming, this method is still more time-efficient than the one described previously if the system size increases to $N_d \approx 500$.

Similar to the previous section, we adopt the notation $\chi_w(T)$, $\chi_m(T)$ and $\chi_f(T)$ for susceptibilities of systems with weak, moderate and full disorder, while $\chi_o(T)$ is the susceptibility of the ordered Mn spin configuration. In Fig. 6.10 we show $\chi_o(T)$ and $\chi_w(T)$ in the upper panel and $\chi_w(T)$, $\chi_m(T)$ and $\chi_f(T)$ in the lower panel for sample size $N = 18$ and $x = 0.092$. The insets focus in on the low-temperature range. In order to reach to bulk limit, for each one of $\chi_w(T)$, $\chi_m(T)$ and $\chi_f(T)$ we have taken an average over 30 different disorder realizations. As previously discussed, the susceptibility for the ordered Mn configuration has a singularity at T_c. For both $T < T_c$ and $T > T_c$, $\chi_o(T)$ decreases monotonically to zero. The disordered configurations, however, have two distinct peaks in the static susceptibilities: one is marking the critical temperature T_c, as in the ordered case. The second peak appears at very low temperatures, $T \ll T_c$, and can be best seen in the insets. With increased disorder, this peak has increased weight and amplitude, and shifts to lower temperatures. This low-temperature peak is due to the quasi-free Mn spins which appear in the disordered samples. These are spins which are far from the regions where the holes are located, and therefore their effective magnetic field H_i [Eq. (3.11)] is extremely small, $H_i \ll k_B T_c$. For temperatures $k_B T > H_i$, they behave like free spins, with a susceptibility $\chi_i(T) \sim 1/T$. The sum of these contributions explains the raise in susceptibility as T is lowered well below T_c. However, as T becomes comparable or less than H_i, these spins order feromagnetically and are frozen out. This results in $\chi \to 0$ as $T \to 0$, and explains the appearance of this low-temperature peak. With increased disorder, there are larger fluctuations in the distribution of holes in the system. As a result, more spins become weakly-interacting, and their effective fields H_i have a broader spectrum extending to lower values, explaining the increase in peak amplitude and its shift to lower temperatures.

The peak appearing in $\chi(T)$ at high temperatures marks the phase transition $T \approx T_c$, as expected. As observed previously [7, 11, 14], increased disorder leads to higher critical temperatures; this trend is clearly seen here, since the second peak in the static susceptibility shifts to higher temperatures for higher levels of disorder. It is important to notice that as disorder is increased the second

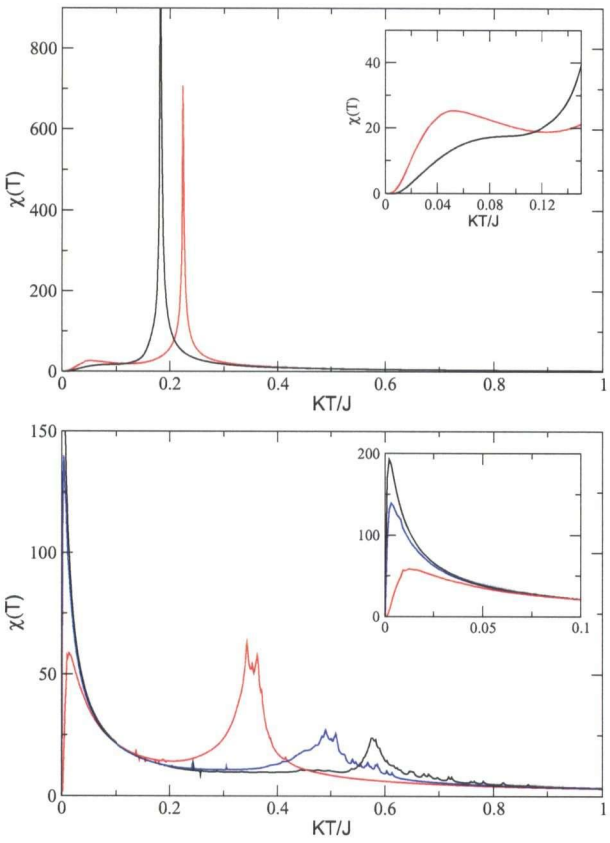

Figure 6.10: Static susceptibility versus temperature. The upper panel shows $\chi_o(T)$ (black line) and $\chi_w(T)$ (red line). The lower panel shows $\chi_w(T)$ (red line), $\chi_m(T)$ (blue line) and $\chi_f(T)$ (black line) for $N_d = 216$, $x = 0.00926$ and $p = 10\%$.

peak broadens and has a smaller magnitude. As we show in the following, the reason for these two effects is due to the formation of clusters. The spins with the largest contribution to this high-T peak are the strongly-interacting spins, from the regions (clusters) where the holes are located with a large probability. Consequently, they have very large effective magnetic fields H_i and order magnetically at high temperatures. With increased disorder, the fluctuations in the local concentration x of Mn spins are larger, implying a wider range of temperatures where the phase transition is taking place.

We now proceed to substantiate these claims based on our numerical data. First it should be noticed that the susceptibilities shown in Fig. 6.10 are av-

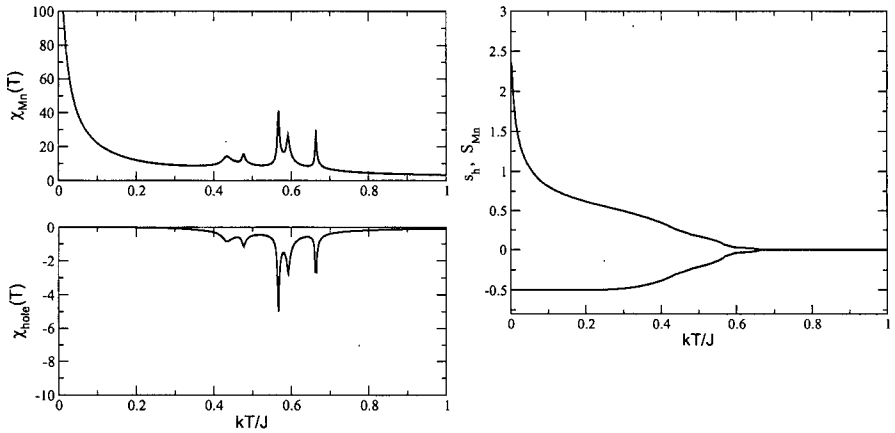

Figure 6.11: Left: the Mn and hole susceptibilities for a *single* disorder realization. Right: average Mn and hole magnetizations for the same disorder realization.$N_d = 512$, $x = 0.00924$, $p = 0.10$.

erages over multiple disorder realizations; the susceptibility $\chi(T)$ for each individual Mn configuration looks rather different. For finite size samples as large as N=24, $\chi(T)$ for each individual disorder realization shows several peaks at a few temperatures in the $T_p < T < T_c$ range, as shown in Fig. 6.11 for a fully disordered configuration (T_p is the temperature below which the holes become fully polarized. The right panel shows the self-consistent average spin ($S_{\rm Mn}$) and hole (s_h) magnetizations for the same Mn configuration). Such peaks appear in both the Mn and hole susceptibilities. They are symmetrically placed and of opposite sign. The peaks in χ_{hole} are smaller (by roughly $p = 10\%$). As explained briefly in section 4.3, even though the external magnetic field is in the opposite direction to the hole polarization, holes become more polarized in the presence of such a field due to their strong anti-ferromagnetic coupling to the Mn spins. This is the reason why χ_{hole} is negative. Furthermore, since holes are fully polarized for $T \leq T_p$, χ_{hole} is zero in this range.

The number of peaks and the temperatures at which they occur in the $T_p \leq T \leq T_c$ range, are different for different disorder realizations. By comparing magnetizations and susceptibilities curves it can be seen that the highest temperature peak in susceptibility always occurs exactly at the mean-field T_c. It is also perceived that these peaks are in fact singularities in the static susceptibility because they become substantially sharper if the self consistency criterion is made more stringent.

The origin of these peaks can be inferred from examining the values $\chi_{\rm Mn}(i)$ at different sites, $i = 1, ..., N_d$, at temperatures where peaks form. We find that the peaks are not due to contributions from all sites $i = 1, ..., N_d$. Instead, each peak is only due to contributions of a distinct group of Mn spins which

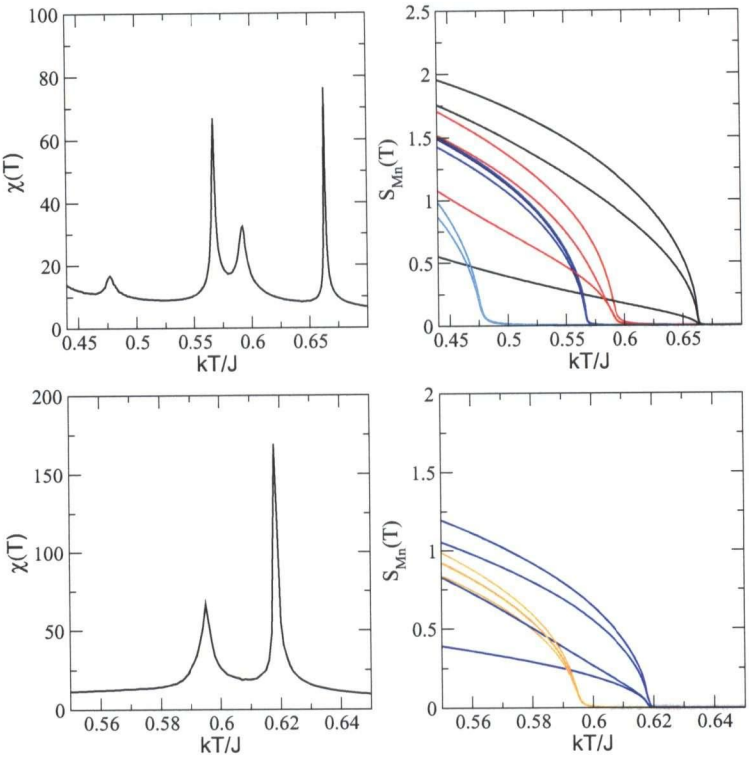

Figure 6.12: Left panels: total susceptibility of two different disorder realizations, near T_c. Parameters are $N = 15$, $x = 0.00934$, $p = 0.10$. Right panels: magnetizations $S_{\rm Mn}(i)$ of spins belonging to different clusters (shown with different colors) which order at temperatures where χ has peaks.

are placed in close spatial vicinity to one another. Such a group of Mn spins can be referred to as a cluster. Mn belonging to a cluster can be identified by examining which of the $\chi_{\rm Mn}(i)$, $i = 1, ..., N_d$ show substantial contribution to each peak of χ. In Fig. 6.12, we show the average magnetizations $S_{\rm Mn}(i)$ for several Mn spins belonging to different clusters (shown in different colors), for two individual full disorder realizations (right panels). The total susceptibilities χ for these two individual Mn configurations are shown in the left panels. We see that the critical temperatures of individual clusters are equal to temperatures where χ has peaks. The critical temperatures of different clusters are directly related to their local densities. Even though it is not shown here, we find that the local hole polarization inside a cluster also becomes finite below its critical temperature. In other words, these peaks mark the temperatures where

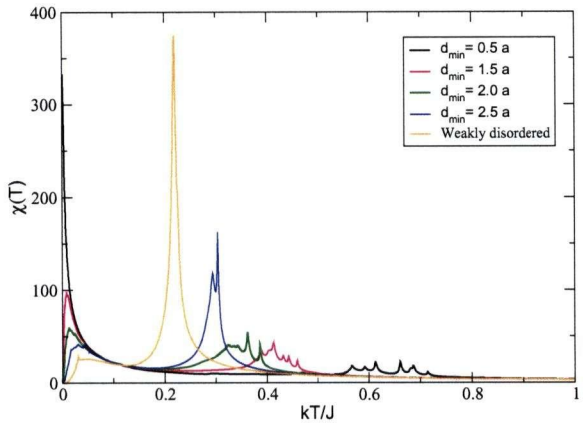

Figure 6.13: Static susceptibility for five types of disorder, characterized by the minimum distance allowed between Mn spins, d_{min}. Each curve is for one disorder realization (not the bulk limit). All samples have $N = 24$, $x = 0.00926$ and $p = 10\%$.

individual strongly-coupled clusters order magnetically.

Strictly speaking, the critical temperature T_c of a sample is not the mean-field temperature where the most strongly-coupled cluster starts to polarize. Instead, several magnetized clusters must appear all throughout the sample, and correlations between their magnetizations must be established (through exchange of polarized holes) before long-range magnetic order develops. This implies that in real samples, this broad peak should extend up to a temperature $T^* > T_c$ below which strong local ferromagnetic correlations, i.e. locally polarized clusters, exist, even though correlations between the magnetizations of different clusters are destroyed by fluctuations.

In Fig. 6.13 we show $\chi(T)$ for five different disorder realizations corresponding to different minimum allowed distances between Mn spins, d_{min}. Parameters are $N = 24$ and $x = 0.092$. The range in which the phase transition occurs as well as the number of peaks becomes smaller for lower degrees of disorder (more homogeneous samples). For the lowest level of disorder, χ_w, results for different individual Mn configurations are very similar to each other and only show one peak at T_c. We have also found that for individual Mn configurations, the number of peaks near T_c increases with system size. For example for full disorder realizations and $x = 0.092$, the number of peaks for $N = 18$, 21 and 24 are usually around 2-3, 4-5 and 5-6 respectively. This is as expected, since larger systems typically have more clusters and a wider distribution of local densities. It follows that for larger sizes, the bulk limit can be reached by averaging over fewer different Mn configuration. In Fig. 6.14 we show χ_f for two sizes $N = 18$ and 21. In order to reach bulk limit for $N = 18$ and 21 curves we have taken an average over 30 and 10 different disorder realizations, respectively. The curves

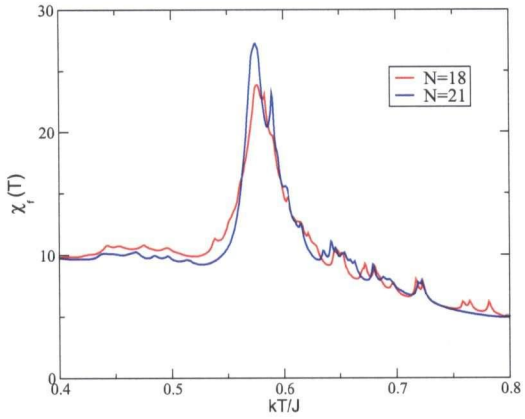

Figure 6.14: $\chi_f(T)$ near T_c for two different sizes N=18 and 21. Curves are in bulk limit, corresponding to averages over 30, respectively 10 disorder realizations. Parameters are $x = 0.00926$ and $p = 10\%$.

we obtain exhibit single broad peaks and are similar to one another, proving that size effects in $\chi_f(T)$ are negligible for $N \geq 18$.

Finally, in Fig. 6.15 we show $\chi_f(T)$ for three different concentrations $x = 0.02$, 0.03 and 0.04 in $4(g\mu_b)^2/a^3$ units. This figure corresponds to individual disorder realizations, however the bulk limit is not hard to visualize. Increased concentration was shown to increases the critical temperature [7], and this is also seen here as the highest temperature peak in χ_f shifts to higher temperatures with increasing x. However, for larger x we find fewer peaks in a smaller range of temperatures near T_c. This is because for higher x the fluctuations in the local concentrations are smaller, reducing the amount of clustering. Therefore in bulk limit we expect to see a decrease in the width of the phase transition peak as we go to higher concentrations.

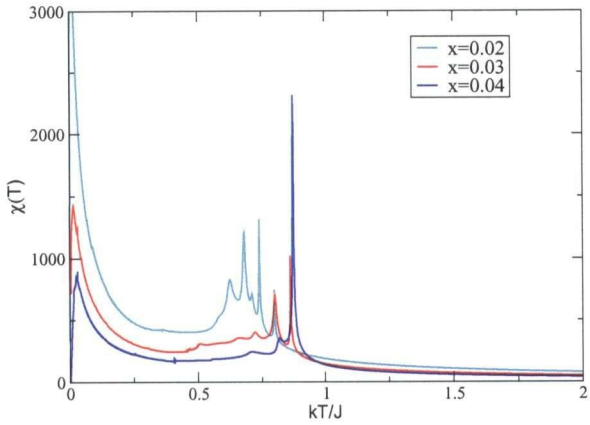

Figure 6.15: $\chi_f(T)$ for three different concentration $x = 0.02$, 0.03 and 0.04. Curves are not in bulk limit. For all curves $p = 10\%$

.

Chapter 7

Summary and Conclusions

In this thesis we studied static and dynamical susceptibilities for DMS at low concentrations, using an impurity band model. Susceptibilities were found to be strongly sensitive to positional disorder of Mn spins.

The transverse dynamical susceptibility $\chi(\vec{q},\omega)$ was considered as a function of energy $\hbar\omega$, for various wave-vectors $\vec{q}$ consistent with the boundary conditions of the Mn supperlattice. The behavior uncovered is in agreement with that expected from the evolution of the spin-wave DOS spectrum: for a fixed value of $\vec{q}$, disorder shifts the weight to lower energies and into a broader peak relative to the sharp peak present in an ordered system at the appropriate spin-wave energy. Disorder also changes the $\vec{q}$ dependence of $\chi(q,\omega)$: for fully disordered Mn configurations and finite $\vec{q}$, the susceptibility becomes roughly independent of the wave-vector.

The static susceptibility was studied as a function of temperature for various levels of disorder. The positional disorder was shown to shift considerable weight to low temperatures and to substantially broaden the high temperature peak signalling the phase transition. The weight at low temperature is linked to the paramagnetic-like contribution of the quasi-free Mn spins. The broadening of the phase transition peak is due to magnetic clustering, since clustering was shown to be responsible for the gradual phase transition over a relatively wide range of temperature (of order of $0.1J$), as different regions of the sample become magnetically ordered. The effects of disorder are less important as the concentration x increases and the local fluctuations in Mn density decrease.

In conclusion, it can be perceived from these results that the inhomogeneous nature of the ferromagnetic state of DMS in the low concentration regime leaves its mark on the magnetic susceptibilities. Its signatures should be clearly seen, and would help validate the impurity band model once measurements of these quantities are performed experimentally.

Bibliography

[1] H. Ohno, J. Magn. Magn. Mat. **200**, 110 (1999).

[2] K.W. Edmonds, K.Y. Wang, R.P. Campion, A.C. Neumann, N.R.S. Farley, B.L. Gallagher, and C.T. Foxon, Appl. Phys. Lett. **81**, 4991 (2002).

[3] A. M. Nazmul, S. Sugahara, and M. Tanaka, Phys. Rev. B **67** 241308(R) (2003)

[4] Y. Ohno, D.K. Young, B. Beschoten, F. Matsukura, H. Ohno, and D.D. Awschalom, Nature (London) **402**, 790 (1999).

[5] H. Ohno, D. Chiba, F. Matsukura, T. Omiya, E. Abe, T. Dietl, Y. Ohno, and K. Ohtani, Nature (London) **408**, 944 (2000).

[6] B. Beschoten, P.A. Crowell, I. Malajovich, D.D. Awschalom, F. Matsukura, A. Shen, and H. Ohno, Phys. Rev. Lett. 83, 3073 (1999).

[7] M. Berciu and R. N. Bhatt, Phys. Rev. Lett. **87**, 107203 (2000).

[8] J. Okabayashi, A. Kimura, O. Rader, T. Mizokawa, A. Fujimori, T. Hayashi, and M. Tanaka, Physica E (Amsterdam) 10, 192 (2001).

[9] A. Van Esch, L. Van Bockstal, J. De Boeck, G. Verbanck, A.S. van Steenbergen, P.J. Wellmann, G. Grietens, R. Bogaerts, F. Herlach, and G. Borghs, Phys. Rev. B **56**, 13 103 (1997).

[10] S. Katsumoto, A. Oiwa, Y. Iye, H. Ohno, F. Matsukura, A. Shen, and Y. Sugawara, Phys. Status Solidi B **205**, 115 (1998).

[11] Mona Berciu and R. N. Bhatt, Phys. Rev. B **69**, 045202 (2004).

[12] K. M. Yu, W. Walukiewicz, T. Wojtowicz, I. Kuryliszyn, X. Liu, Y. Sasaki and J. K. Furdyna, Phys. Rev. **B 65**, 201303(R) (2002).

[13] A.K. Bhattacharjee and C.B. la Guillaume, Solid State Commun. 113, 17 (2000)

[14] M. P. Kennett, M. Berciu and R. N. Bhatt, Phys. Rev. **B 66**, 045207 (2002).

[15] Mona Berciu and R. N. Bhatt, Phys. Rev. B **66**, 085207 (2002).

[16] G. Zarand and B. Janko, Phys. Rev. Lett. **89**, 047201 (2002).

[17] L. Brey and G. Gmez-Santos, Phys. Rev. B **68**, 115206 (2003)

[18] C. Zhou, M.P. Kennett, X. Wan, M. Berciu and R.N. Bhatt, Phys. Rev. B **69**, 144419 (2004).

[19] R. N. Bhatt, Phys. Rev. B **24**, 3630 (1981); **26**, 1082 (1982).

[20] S. Sanvito and N. A. Hill, Phys. Rev. **B** 62, 15553 (2000); S. Sanvito, P. Ordejon and N. A. Hill, Phys. Rev. **B** 63, 165206 (2001).

[21] M. Berciu and R. N. Bhatt, Phys. Rev. Lett. **90**, 029702 (2003).

[22] J.-P. Blaizot and G. Ripka, *Quantum theory of finite systems* (MIT Press, Cambridge, Mass., 1986).